General Disclaimer

One or more of the Following Statements may affect this Document

- This document has been reproduced from the best copy furnished by the organizational source. It is being released in the interest of making available as much information as possible.

- This document may contain data, which exceeds the sheet parameters. It was furnished in this condition by the organizational source and is the best copy available.

- This document may contain tone-on-tone or color graphs, charts and/or pictures, which have been reproduced in black and white.

- This document is paginated as submitted by the original source.

- Portions of this document are not fully legible due to the historical nature of some of the material. However, it is the best reproduction available from the original submission.

Produced by the NASA Center for Aerospace Information (CASI)

DRI

Dansk Rumforskningsinstitut
Danish Space Research Institute

Observation of a Westward Travelling Surge from Satellites at Low, Medium and High Altitudes

Eigil Ungstrup, R. D. Sharp, C. A. Cattell, R. R. Anderson,
R. J. Fitzenreiter, D. S. Evans, and D. N. Baker

Lyngby 1984

OBSERVATION OF A WESTWARD TRAVELLING SURGE FROM SATELLITES AT LOW, MEDIUM AND HIGH ALTITUDES.

Eigil Ungstrup[*] and R.D. Sharp
Lockheed Palo Alto Research Laboratories, Palo Alto, CA 94304

C.A. Cattell
Space Sciences Laboratory, University of California,
Berkeley, CA 94720

R.R. Anderson
Department of Physics and Astronomy, University of Iowa,
Iowa City, IA 52242

R.J. Fitzenreiter
NASA Goddard Space Flight Center, Laboratory for Extraterrestrial
Physics, Greenbelt, MD 20771

D.S. Evans
Space Environment Laboratory, NOAA, Boulder, CO 80303

D.N. Baker
Los Alamos National Laboratory, Los Alamos, NM 87545

May 1984

[*] Permanent address: Danish Space Research Institute,
Lundtoftevej 7, DK-2800 Lyngby, Denmark.

ABSTRACT

The westward travelling surge from a particular substorm on
April 20, 1981 was observed by satellites at low, medium and
high altitudes and the combined observations show new details
about how plasma is energized during substorms.

Both the observations from the low-altitude satellite NOAA-6
and from ISEE-1 at 10300 km altitude show that electrons are
accelerated by an electric field with a potential drop of 10-15
keV and the ISEE-1 observations show that this potential drop
occurred beyond 10300 km altitude. Immediately after the surge
a very dense electron population was observed at ISEE-1 where
the hot electrons were trapped between a magnetic mirror below
and an electric mirror above the satellite. This hot electron
population decayed slowly over a period of 3 to 4 minutes during
which period there was very strong electrostatic and
electromagnetic wave activity.

Immediately after the current sheet or current filament associated
with the surge passed over ISEE-1 there was a sharp onset of
conic ion beams. The ions were heated transversely at and below
ISEE-1 to a depth of about 1 R_E below the satellite. The
transversely heated ions were apparently lifted out of the
lower magnetosphere by the $\mu \cdot$ grad B force and the heated ions
passed out beyond ISEE-1 in $\sim$4 minutes for protons and $\sim$15
minutes for oxygen ions.

When the surge passed the field line connected to the
geostationary satellite 1976-059 there was an immediate onset
of high fluxes of energetic ions > 145 keV and electrons >
30 keV. In addition to the usual "injection" picture, the
sudden occurrence of energetic ions at the geostationary orbit
might be explained in the following way: the transversely heated
ions may be moved towards the equator by the $\mu \cdot$grad B force
in the Earth's magnetic field. When the ions with initial energies
of a few hundred eV enter the electric field region above ISEE-1

they may be accelerated to an energy of 10-15 keV. We know
from magnetograms that the event occurred simultaneously in
both hemispheres, and in the region near the geomagnetic equator
we thus expect two oppositely directed ion beams. These ion
beams could interact with the ambient plasma at high altitudes
near the equator (or with each other) and cause plasma
instabilities that tend to thermalize the ion population. We
would thus expect to have a sudden occurrence of hot ($\sim$10-15
keV) ion plasma in the equatorial region and it may be the
tail of this distribution that is observed by the geostationary
satellite. The bulk of this hot plasma may to begin with be
confined to equatorial regions by the electric potentials,
but when the fields decay the hot ions will be distributed
along the field lines.

1. INTRODUCTION

An interesting and important feature near the onset of magnetospheric substorms is the westward travelling surge and poleward expansion. The Westward Travelling Surge (WTS) occurs during the expansion phase of substorms and it was first recognized by Akasofu et al. (1965, 1966), and studied by Akasofu and Meng (1967a,b,c,d), and Akasofu (1968) based on all-sky-camera and magnetometer observations of substorms. Later the westward travelling surges have been studied by a number of different methods both from the ground, and from rockets and satellites.

Rostoker and Kisabeth (1973), Kisabeth and Rostoker (1974), and Wiens and Rostoker (1975) studied the development of the westward electrojet with observations from the University of Alberta meridian line of magnetometers and all-sky-camera data and found that the expansive phase of substorms is not a continuous process but involves a series of poleward and westward jumps of the westward electrojet. They concluded that the westward electrojet develops in a succession of jumps at intervals of about 10 minutes in such a way that each new electrojet appears to the northwest of the previous one.

Opgenoorth et al. (1980, 1983), Tighe and Rostoker (1981), Baumjohann et al. (1981), and Inhester et al. (1981) expanded the model of the westward travelling surge to include a strong upgoing field aligned current at the head of the surge. This field aligned current system is fed by the westward electrojet. Tighe and Rostoker show the field aligned current as a sheet current whereas the other papers seem to favor a field aligned current filament but as the north-south extent of the surge is comparable to its height and to the distance between the magnetometers in the current observatory system then the spatial resolution is rather poor and the results are not conclusive.

Akasofu et al. (1969) find an absence of hydrogen emission in the westward travelling surge together with an electron flux of 4.10^9 cm^{-2} s^{-1}, which also suggests that the electron flux in a westward travelling surge constitutes an upward field aligned electric current.

Westward travelling surges have also been studied by rocket experiments. The experiment by Rème and Bosqued (1973) show a hardening of the electron spectrum in the surge and also that there is a peak in the differential electron spectrum near 20 keV. A similar result, but with the energy peak closer to 10 keV, was obtained by Sandahl et al. (1980) and Marklund et al. (1983).

Observations of westward travelling surges from low altitude satellites have been reported by Meng et al. (1978). Their observations support the rocket observations mentioned above in that they find a strong increase of the electron precipitation and a hardening of the electron spectra. The differential energy spectra were at times unusually flat from 0.2 to at least 20 keV and at other times showed a spectral peak at 8 keV or higher energies.

A westward travelling surge was observed by Mende et al. (1972) on the geostationary satellite ATS-5. They observed a strong increase in the fluxes of energetic ions and electrons at the substorm onset which was followed by a westward travelling surge. The sudden increase of energetic particle fluxes at geostationary orbit is now used as a signature of substorm onset in many magnetospheric studies (Baker et al., 1981 and references therein).

We have identified an event observed by several instruments on the satellite ISEE-1 on April 20, 1981 at 2348 UT as the signature of a westward travelling surge. This identification is confirmed by ground based magnetometer observations which show that a fairly typical substorm began at 2330 UT and that the WTS from this substorm passed the area conjugate to ISEE-1 at the right time. The ground magnetometer observations are discussed in section 2.

The westward travelling surge was also observed by the satellite NOAA-6 at 815 km altitude at 2332:45 UT and by the satellite 1976-059 in geostationary orbit at 2333:05 UT. Field line tracing in a model of the Earth's magnetic field show that NOAA-6 and 1976-059 were conjugate at the time they observed the surge. The observations from these satellites are discussed in section 3.

ISEE-1 was at 10300 km altitude when the discontinuity associated with the surge passed over this satellite. From ISEE-1 we have a very comprehensive set of observations that shows new and interesting features of magnetospheric discontinuities. The observations made from ISEE-1 and the other two satellites are shown in Table 1 and the observations from ISEE-1 are discussed in section 4.

Finally in section 5 we discuss the combined observations in an attempt to understand the implications of westward travelling surges for magnetospheric physics.

TABLE 1

SATELLITE OBSERVATIONS

Satellite	Altitude	Observations
NOAA-6	815 km	Electrons 0.3 to > 300 keV Ions 0.3 to > 2.5 Mev
ISEE-1	10300 km	DC electric fields DC magnetic fields AC electric fields 5 Hz-400 kHz AC magnetic fields 5 Hz-10 kHz Electrons 100-7000 eV Ions 0.2-17 keV O^+ , H^+
1976-059	35800 km (geostationary)	Electrons $\geq$ 30 keV Ions $\geq$ 150 keV

2. GROUND OBSERVATIONS AND GEOPHYSICAL CONDITIONS

The event was observed by magnetometers and riometers in Iceland, Greenland, and Eastern Canada, and the associated partial ring current was evident in the magnetogram from San Juan, Puerto Rico. In Figure 1 we show the horizontal component of the Earth's magnetic field from a selection of observatories. On the map in Figure 2 the onset times of the event at the different observatories and at the satellites NOAA-6, 1976-059 and ISEE-1 are marked at the positions of the observatories and at the satellite conjugate points. The onset times and types of observations are in addition summarized in Table 2. The San Juan magnetogram at the top of Figure 1 initially shows a depression of the horizontal component. At 2329 UT the field starts to recover indicating a positive bay development (e.g. Rostoker et al., 1980). This is followed immediately by the sharp onset of a substorm at Ottawa and St. Johns in Canada and at Leirvogur in Iceland. In the next 20 minutes the disturbance moves northwestward across Labrador and Hudson Bay until the last observation at Churchill at 2349 UT. At that time the mid-latitude magnetic field, as judged from the San Juan magnetogram, is back to the level it had before the ring current started to build up around 19 UT. The absence of signatures at magnetic observatories west of Churchill suggests the possibility that the energy stored in the ring current and/or magnetotail is spent by the time the disturbance reaches Churchill and that no more free energy is available to drive the disturbance.

Owing to the time of the year that the event occurred we have no optical auroral observations, but the progression of the event seen in ground magnetometer records strongly suggests that the event is a westward traveling surge associated with a substorm (Akasofu et al., 1966; Akasofu and Meng, 1967a,b,c,d; Akasofu, 1968)

TABLE 2

APRIL 20, 1981   EVENT ONSET TIMES

San Juan, Puerto Rico	2329 UT	Mid-latitude positive bay
St. Johns, New Foundland	2330 UT	Substorm onset
Ottawa	2330 UT	Substorm onset
Leirvogur, Iceland	2330 UT	Substorm onset, sudden
NOAA-6	2333 UT	Onset particle precip.
Satellite 1976-059	2333 UT	Onset energetic part.
Narssarssuaq, Greenland	2333 UT	Substorm onset
Great Whale River, Canada	2337 UT	Magnetic impulse
ISEE-1	2348 UT	Onset waves/particles
Fort Churchill, Canada	2349 UT	Magnetic impulse

The apparent velocity of the disturbance in the ionosphere can be determined from the onset times, although with some uncertainty. Between the NOAA-6 footprint and Great Whale River the velocity was approximately 2.7 km/s and between Great Whale River and Churchill the velocity was 1.5 km/s.

The magnetosphere was moderately-to-strongly disturbed in the period surrounding the event. Kp was 6- on April 20, 21-24 UT and 4+ on April 21 00-03 UT. The hourly equatorial Dst values from 20 UT on April 20 to 02 UT on April 21 were: -90, -101, -101, -84, -67, -62.

The interplanetary magnetic field at ISEE-3 is shown in Figure 3. It was southward from 2136 until 2210 UT, northward until 2235 UT, southward from 2235 to 2245 UT and then northward until the following day. Assuming a propagation time of 50 to 60 minutes from ISEE-3 to the Earth, it would be the southward interplanetary magnetic field from ~2235 to ~2245 UT that is associated with the substorm at 2330 UT (e.g. Fairfield et al., 1981; Baker et al., 1981).

3. SATELLITE OBSERVATIONS FROM NOAA-6 AND 1979-059

Observations from NOAA-6

NOAA-6 is in a sun-synchronous dawn-dusk 98° inclination orbit
and travels northward at 815 km altitude over Labrador immediately
after the onset of the substorm on April 20, 1981 as discussed
in section 2.

The NOAA-6 particle instrument (Hill and Evans, 1981) includes
sensors which measure ion and electron fluxes from 0.3 to >300
keV. Below 20 keV the measurements are made by a conventional
electrostatic analyzer-channel multiplier detector system.
Observations are made separately for ions and electrons at
each of two pitch angles, both well within the atmospheric
loss cone at auroral latitudes. Data processing within the
instrument converts the sensor response during an energy sweep
from 0.3 to 20 keV to a measure of the integrated directional
energy flux carried into the atmosphere by these particles.
The sensitivity of the instrument allows directional energy
fluxes from 0.01 to 100 erg cm^{-2} s^{-1} sr^{-1} to be reliably measured
within a 2 second integration period.

In addition to the energy flux parameters, the energy band
within which the particle energy flux maximized and the sensor
response within that energy band are transmitted for both
electrons and ions for each 2 second integration period. These
data provide the "characteristic" or average energy of the
particles and the particle flux at that energy. At a low duty
cycle (3 energy sweeps of 16 for each of the two particle species
at each of the two pitch angles) the particle count rates in
4 energy channels (of 11) are telemetered. In those cases
for which this additional information is available, it is possible
to reconstruct a detailed energy spectrum over the range 0.3->100
keV. The reconstruction technique uses the measurements of
the integrated energy flux (0.3-20 keV), knowledge of the particle
energy and intensity at the maximum in the spectrum, and the
>30 keV particle observations as constraints on the shape of

the energy spectrum and the particle intensities at energies that were not telemetered. Two of such reconstructed spectrums are shown in Figure 4.

The precipitated energy flux carried to the atmosphere by ions and electrons within the 0.3-20 keV energy range is shown in Figure 5 together with the characteristic energy of the electrons. The precipitating energy flux starts to increase at 2332:10 UT, reaches 1 erg cm^{-2} s^{-1} at 2332:30 UT and peaks at 199 erg cm^{-2} s^{-1} at 2332:50 UT. The two nulls in the precipitated energy flux at 2332:55 and 2333:35 UT may be caused by saturation of the instrument.

At energies above 30 keV, the measurements of protons and electrons are made by solid state detector telescopes. The detectors are mounted in pairs with one pair viewing radially outward along the Earth-satellite vector so as to measure precipitating particles and the other pair mounted nearly perpendicular to the first to detect particles which would magnetically mirror at altitudes above 200 km (i.e. trapped). One detector in each pair is sensitive to protons the other to electrons. Pulse height analysis is used to identify energy. More details about the instruments is found in Lyons and Evans (1984).

Precipitation of energetic ions start around 2331:40 UT and around 2332:00 UT the precipitation of both electrons and ions above 30 keV increase sharply as seen in Figure 6. At this time NOAA-6 is at a dipole latitude of 59.3° and an invariant latitude of 60.6°. At 2332:50 UT when the satellite is at 63.8° invariant latitude we observe a dip in the precipitation of both energetic ions and electrons. This dip is most pronounced for the ions and in Figure 5 it is seen that the minimum in energetic ion precipitation almost mirrors the maximum in precipitation of low energy electrons. The trapped proton flux in the energy range 30-80 keV decreases by a factor of 30 and the low pitch angle (precipitating) flux by a factor of 60. At the same time the low energy particle spectrometer shows peaked electron spectra as shown in Figure 4. The peaked electron spectra suggests an electrostatic acceleration of the electrons (Evans, 1974). This supposition is supported by the suppression in count rates for energetic ions. A field aligned electric

field directed away from the Earth at some altitude above the satellite will inject a beam of field aligned electrons toward the Earth, but it will also decelerate the ions and lift their mirror points and thus reduce the energetic ion flux observed by a low altitude satellite as NOAA-6.

In Figure 6 we show the greater than 30 keV electron count rates for both the precipitating and trapped pitch angles. It is interesting to note that the count rate of mirroring electrons ($\emptyset = 90^{\circ}$) is almost constant from 2330:30 UT and until about 2332:55 UT. The precipitating electrons are first observed above threshold at 2332:00 UT but the count rate for these electrons is also low until 2332:55 UT. We can thus conclude that the first strong injection is caused by low energy electrons. After the first low energy electron injection the count rate of energetic electrons increase by about two orders of magnitude and remains high until the end of the main event at 2333:40 UT.

In Figure 7 we show the energy flux averaged over 1° latitude intervals as function of geomagnetic latitude. We see that the energy flux peaks at 80 erg cm^{-2} s^{-1} at 61° dipole latitude. This is a very low latitude for such a strong event and it suggests that the event took place at the inner edge of the plasma sheet or possibly even on closed field lines inside the magnetosphere. The fact that the trapped particle fluxes return to the pre-event levels after the event and first drop of at 2333:40 UT when the satellite is at 66° invariant latitude (5.2° dipole latiude) supports this hypothesis.

Observations from the 1976-059 geostationary satellite.

As shown in the map in Figure 2 the geostationary satellite 1976-059 located at 64° W was almost conjugate to NOAA-6 at the time of the above observations. This spacecraft has Los Alamos National Laboratory energetic particle sensors onboard (e.g. Baker et al., 1981, and references therein). Figure 8 shows the 1976-059 observations of electrons between 30 and 0 keV and ions between 145 and 560 keV.

As described previously, and as shown in Figure 1, the latter portion of April 20, 1981 was geomagnetically disturbed. Several substorm particle injection events were observed at geostationary orbit both by spacecraft 1976-059 (Figure 8) and by spacecraft 1977-007 which was also at 6.6 R_E ~9 hours east of 1976-059.

Energetic particle intensities at satellite 1976-059 show a progressive decrease for approximately 1 hour prior to the 2330 UT substorm onset. Between 2310 and 2333 UT the particle intensities at geostationary orbit are near background levels suggesting a complete flux dropout. This type of dropout followed by a simultaneous several orders-of-magnitude increase of electrons and ions of all energies seen by 1976-059 at 2333 UT is the signature of a magnetospheric substorm at this local time at geostationary orbit (Baker et al., 1982)

4. ISEE-1 OBSERVATIONS

Magnetic Field observations.

The spin-averaged Z-component of the magnetic field from the UCLA fluxgate magnetometer (Russell, 1978) is shown in Figure 9a. The main field was primarily in the -X, -Y direction until 2342 UT, and then in the -Y direction. The total change around 2348:30 UT in the B_x and B_z magnitude is 240 and 270 nT respectively while there is hardly a noticeable change in the B_y magnitude. The magnetic variations can be interpreted as resulting from field aligned currents. We see thus that ISEE-1 passes a sequence of current sheets or filaments of which the biggest occurs between 2348:20 and 2348:40 UT and causes a change of 230 nT in the Z-component of the magnetic field. A positive change in B_z corresponds to a current out of the ionosphere and the main disturbance of the magnetic field is thus caused by an outgoing field aligned current. The largest electron fluxes discussed below are associated with the beginning of current flow out of the ionosphere. There is no clear correlation between other features in the electrons and the currents.

DC Electric Field observations

The electric field data were obtained from the University of California, Berkeley double probe experiment (Mozer et al., 1978) which makes a measurement of the electric field along the boom direction 8 times per second, from which a measurement of the two components in the spin plane can be determined by least squares fitting of the data over one spin period (3.04 seconds). Only the raw data are presented here, for two reasons: (1) large variations in the field occurred on a time scale less than three seconds, and (2) largest component in the auroral zone at dusk is typically in the north-south direction (Mozer et al., 1980), which maps at ISEE-1 altitudes to a field along the spin axis. Since this component is not measured,

and cannot be reliably determined using $\overline{E} \cdot \overline{B} = 0$ since B_y/B_z is large and any error in the measurement of the electric field is multiplied by that factor, presentation of the spin-averaged data would not provide any additional information.

During the period of interest (2330 to 2400 UT), there were two regions of large variable electric fields, as can be seen in Figure 9b. The first, which occurred before the main event, extended from 2335:00 to 2338:30 UT as the satellite moved from $L = 6.5$ to $L = 7.5$ at an altitude of 1 R_E and local time of 1600. The fluctuations reached a magnitude of 100 mV/m. Enhancements of ~2 orders of magnitude were observed by the low frequency filters (center frequencies of 4, 32 and 256 Hz), which are not shown here. The largest fluctuations occurred at the same time as an oxygen conic was observed.

The electric field then remained roughly constant (except for long period fluctuations which are correlated with quasiperiodic pulsations in the electron density, see below) until the second region of large variable fields at 2348 UT, which lasted for several minutes. At this time electric fields up to 250 mV/m were observed. This period is shown in greater detail in Figure 10. The largest electron fluxes (which are discussed below) occur at the edge of the region of strong electric fields 2348:30 UT. There is no other clear relationship between the observed electrons and ions and the short time scale changes in the electric field. After 2351 UT, the average electric field magnitude returns to the pre-discontinuity value, but remains more variable.

Ion mass spectrometer observations

The ion mass spectrometer (IMS) has been described by Shelley et al., (1978). It was in the fast auroral mode during this event. This mode has a high time resolution since it steps through only 8 energy steps and two species, O^+ and H^+. The energy steps are approximately logarithmically spaced at: 0.22, 0.42, 0.63, 1.36, 2.26, 4.3, 9.3 and 17.0 keV. The instrument stays on each energy step and species for a full spin period (3.04s), and since the Earth's magnetic field was nearly in the spin plane of the satellite during the event, we obtain

the full pitch angle distribution of the ions.

Figure 11 shows the data acquired during the period of interest in the form of pitch angle distributions of oxygen and hydrogen ions in the energy range 0.2 to 17 keV. It takes 52 s to accumulate data for one pair of frames (O^+ and H^+) in Figure 11. The data sampling sequence starts with oxygen and then hydrogen on the lowest energy step, progresses up in energy and ends with a four second sampling of background fluxes. A flux measurement at a single energy and angle is acquired every 62.5 ms in which time the spacecraft rotates approximately 7.5^o.

On April 20, 1981 the IMS was turned on at 2336 UT as ISEE-1 moved out from perigee. At 2338 UT a conical distribution of oxygen with pitch angle close to 90° was observed, simultaneously with a quasi-isotropic population of hot protons. This event was only observed in one frame, which means that it lasted less than 100 s, and for the next 10 minutes there were very few hot ions around ISEE-1. This conic occurred at the same time as the first period of large and variable electric fields discussed above. The counts per interval in the period 2338 to 2348 UT were mostly in the range 0 to 2 (i.e. near background) except that there was a tendency for slightly higher counts for oxygen at angles close to 180°. This can be seen in frames a and c to the left in Figure 11, which are representative of this ten minute period before the start of the main event.

TABLE 3

Ion Mass Spectrometer Observations

Time Interval UT	Ion	E keV	Flux /(cm²s sr keV)	Pitch Angles degrees	
2348:45 – 2349:37	O+	0.2	1.2+8	072–082	125–141
	H+	0.2	1.1+7	085–108	
	H+	0.4	2.7+7	097–132	108–138
	O+	0.6	1.2+8	090–105	093–115
	H+	0.6	1.2+7	104–130	095–140
	O+	1.4	1.3+7	098–107	
	H+	1.4	1.5+6	110–122	
	O+	2.4	9.4+5	095–110	095–118
	H+	2.4	1.8+6	104–125	090–130
2349:37 – 2350:29	O+	0.2	2.2+8	115–136	111–142
	H+	0.2	5.2+7	133–160	117–177
	O+	0.4	1.6+8	095–107	160–175
	H+	0.4	4.6+7	085–110	104–145
	O+	0.6	4.6+6	092–102	
	H+	0.6	1.5+6	110–133	110–128
	H+	1.4	2.4+5	115–120	
2350:29 – 2351:21	O+	0.2	1.6+8	112–138	120–145
	H+	0.2	5.4+7	123–145	128–150
	O+	0.4	4.0+7	116–131	111–132
	H+	0.4	2.0+6	135–149	143–150
	O+	0.6	3.0+6	118–127	115–135
2351:21 – 2352:13	O+	0.2	1.7+8	110–130	126–145
	H+	0.2	6.0+6	137–160	137–163
	O+	0.4	2.2+7	125–138	125–138
	O+	0.6	8.2+6	126–136	136–147
2352:13 – 2353:05	O+	0.2	9.7+6	116–129	136–146
	O+	0.4	1.6+6	134–143	141–149
2353:05 – 2353:57	O+	0.2	1.3+7	119–136	128–152
2353:57 – 2354:49	O+	0.2	7.6+6	135–152	137–153
2354:49 – 2355:41	O+	0.2	2.2+5	150–158	
2355:41 – 2356:33	O+	0.2	1.7+8	138–155	146–163
	O+	0.4	2.5+5	142–160	
2356:33 – 2357:25	O+	0.2	1.0+8	131–148	152–167
	O+	0.4	3.1+5	154–159	
2357:25 – 2358:17	O+	0.2	3.3+7	122–155	143–163
2358:17 – 2359:09	O+	0.2	3.4+6	137–155	148–160

The event starts in the ions at 2348:28 UT when the IMS observes
an increase in the flux of 4.3 and 9.3 keV protons. These protons
have a wide angular distribution as can be seen in Figure 11d.
In the following six pairs of frames, Figure 11e to 11n, one
sees clearly the conical distributions of ions at several
energies, where the ion flux peaks at a pitch angle between
90° and 180°. An upgoing field aligned beam would appear as
a peak in the ion flux at 180°. All the conics during the
first 11 minutes of the event are listed in Table 3. In this
table we give the peak fluxes and the pitch angle range at
half maximum flux for both oxygen and hydrogen at all energies
for which conical distributions were observed. From this table
it is seen that the hydrogen peaks moved relatively quickly
from 90°-100° up to 140°-160°, whereas the oxygen peaks increased
their pitch angles more slowly.

A close examination of Figure 11e to 11n or of Table 3 shows
that on occasion some conics are missing. Ion conics are only
observed on the lowest energies and if one or more conics in
a sequence are missing then a likely explanation for the missing
conic(s) is time variations. Thus drop-outs can only be identified
if they occur when the ion mass spectrometer is scanning the
lowest energies and only if they last more than half a spin
period. Our information on time variation in the ions is thus
incomplete but there are some interesting drop-outs during
the first three frame pairs shown in Figure 11e to 11j. This
Figure, or Table 3, only shows the approximate times of the
missing conics. More exact times can be found in a computer
listing of the raw data from the instrument. (We have also
used these listings to determine the exact start of the ion
event noted above). We find one drop-out of conical distributions
between 2348:48 and 2348:55 UT and another at 2349:45 to 2349:47
UT. We will later compare these drop-outs to the fine structure
found in other observations on ISEE-1.

The temperature of the conic distribution for each species
can be derived from the phase space density as function of
energy when the time variations are small. For the period 2348:45
to 2349:37 UT we find a temperature of 265 eV for the oxygen
and 235 eV for the hydrogen. The next frame cannot be used
because of time variations in the ion fluxes. However, the

next two periods (2350:29 to 2351:21 and 2351:23 to 2352:13
UT) show relatively stable distributions and give a temperature
of 80 eV for the O^+. Only the first of the two periods (2350:29,
to 2351:21 UT) can be used for the H^+, and it gives a temperature
of 58 eV. Note that at this time the source region ("mirror
point") of the H^+ has moved far down the field line, and is
much lower than the source region of the O^+ and the temperature
is therefore not necessarily a measure of the temperature of
the H^+ ions at the same location as the observed O^+ ions.

Electron observations

The electron data were obtained by the electron spectrometer
experiment (Ogilvie et al., 1978) which was operating in a
mode measuring electrons from 0.1 to 7.1 keV. In Figure 12a
and 13a are contour plots of parallel phase space density of
the electrons for this energy range. Parallel velocity (positive
along the Earth's magnetic field) is along the ordinate and
time along the abscissa. Three levels of the natural logarithm
of parallel phase space density are contoured in Figure 12a:
ln F = -20 (inner closed contours), ln F = -24 (heavy line),
and ln F = -26 (outer light line). In Figure 13a, successive
contoured levels of ln F differ by unity. The contours are
labelled by -ln F. The data used to produce these contours
are measured over the time of a spacecraft rotation period
of 3.04 seconds and are repeated each 9.125 seconds.

The start of strong pulsations in the phase space distribution
at 2333 UT can be seen in Figure 12a which shows the electron
data for the period from 2330 to midnight UT. The observed
pulsation period (~70 s) is in the Pc4 range. The pulsations
are very strong to begin with but decrease in amplitude until
the sharp discontinuity between 2348:24 and 2348:33 UT. The
single conic of 0.22 keV oxygen mentioned above occurred during
the last of the strong pulsations at 2337:30 UT. During the
ten minute period preceding the discontinuity when the ion
mass spectrometer observed only background fluxes, the electron
phase space density was very low for parallel velocities above
10^9 cm/s.

The phase space density around the discontinuity is shown on an expanded time scale in Figure 13a. In this figure one sees the last of the Pc4 pulsations at 2348:06 UT followed by the change in the electron distribution function marking the discontinuity between 2348:24 and 2348:33 UT. The onset of the discontinuity in the electron data and the observation of the first hot ions coincide to within the 9.125 s cycle time of the electron measurements. At the discontinuity the parallel phase space density jumps by e^6 to e^7 corresponding to a change by a factor of ~400 to ~1100, depending upon energy.

In Figure 14 the two-dimensional phase space densities for each 9.125 s (every third spin period) from 2348:23 to 2348:41 UT are plotted. The three upper frames show the two-dimensional phase space density for the three observations closest to the discontinuity. The magnetic field is directed to the right in the figure and the contours are labelled by the negative natural logarithm of the phase space density. Velocity units for $v_{\parallel}$, $v_{\perp}$ is 10^8 cm/s or 1000 km/s. Before the discontinuity the electron distribution is rather isotropic but after the discontinuity the distribution is strongly elongated along the Earth's magnetic field. In the lower frames we have shown the natural logarithm of the parallel phase space density. The curve with the heavy dots assume that the phase space density is constant across the loss cone whereas the curve with the light dots excludes the loss cone contributions.

We have also used these observations to determine the electron density. The zero'th order moment of the measured electron distribution functions in the range 0.1 keV $\leq$ E $\leq$ 7.1 keV. Figure 15 shows that the electron density jumps from less than one per cc to about 24 cm^{-3} at the time of the discontinuity. The electron density remains high (between 4 and 13 cm^{-3}) for about 3 minutes after the discontinuity.

Wave Observations

Observations of electrostatic and electromagnetic waves in the range from 5.6 Hz to 311 kHz were made by the University of Iowa plasma wave experiment (Gurnett et al., 1978). The wave spectrum from 0.1 to 400 kHz is shown in Figure 16. Between

2330 and 2400 UT strong auroral kilometric radiation (AKR) in the frequency range from 100 to 400 kHz occurred. At 2348 UT there was a sharp increase in the level of AKR simultaneous with an increase in the level of waves in the whistler mode range below 50 kHz. A more detailed picture can be seen in Figure 12b where the amplitude spectrum as a function of time is plotted for selected frequencies in the range from 5.6 Hz to 311 kHz for the half hour of interest. Between 2334 and 2338 UT there were strong signals at all frequencies at the same time that the strong pulsations in the phase space density of electrons, the first region of large DC electric fields, field aligned currents and a conical distribution of oxygen was observed. This was followed by a period of 10 minutes when the signals below 562 Hz (~ the lower hybrid resonance frequency) were very low. During that period the phase space density of the electrons was low and the ion mass spectrometer recorded near background levels.

At 2348:20 UT the wave intensity started to increase in all channels. At 2348:28 UT the lowest frequency channels jumped almost to saturation, remaining high for 150 to 180 s. This is emphasized further in Figure 17, where calibrated signals are shown on an expanded time scale. The slow increase in wave intensity followed by a sudden jump is seen very clearly at 56.2 Hz. However, some of the higher frequencies notably 562 Hz, seem to have precursors starting at 2348:05 UT, or possibly even earlier at the higher frequencies. The wave amplitude increased by up to 3 orders of magnitude at the onset of the event as shown in Figure 18.

A close examination suggests that the variations in wave intensity were associated with variations in phase space density of electrons and the drop-outs of ion conics at 2348:48 UT. Since at later times the correlation was more uncertain, these near simultaneous variations may have been a coincidence. The wave intensity at 562 Hz and higher frequencies is quite variable and peaks of 40 to 50 dB lasting 1 to 2 seconds are protruding from the base level of wave intensity.

The two lowest channels, 5.6 and 10 Hz, are almost saturated for a period of 80 s beginning at 2348:30 UT. For the 5.6 Hz channel this corresponds to a level of 10^{-4} V^2 m^{-2} Hz^{-1} or

an amplitude of 13 mV/m for the 1.7 Hz bandwidth of the 5.6 Hz channel. 5.6 Hz is the second harmonic of the oxygen ion cyclotron frequency at the spacecraft. The wave intensity falls steeply with frequency and is down almost three orders of magnitude at 56 Hz which is the channel closest to the hydrogen cyclotron frequency of 45 Hz. From the shape of the spectrum it is reasonable to assume that the wave intensity would be even higher at the oxygen cyclotron frequency of 2.8 Hz than it was in the 5.6 Hz channel. It thus seems that the waves present were probably oxygen cyclotron waves. Unfortunately we are not able to check this point because of the lack of measurements below 5.6 Hz. The University of California waveform sampling was on during the event, but during the period with intense wave activity it was saturated.

4. DISCUSSION

The following topics will be addressed using the observations described above: (1) motion of the discontinuity; (2) the electric potential and current structure of the event; (3) the energy source and flow; (4) wave-particle interactions; and (5) particle acceleration. The model in Figure 19 will be used to organise the discussion of the observations.

ISEE-1 was moving away from the Earth with an Eastward velocity of about 4.5 km/s, which projects along the magnetic field to a velocity in the ionosphere of 0.85 km/s. It was situated on an L-shell with L ~ 7.3. The discontinuity was moving westward with an apparent ionospheric velocity decreasing from 3.3 km/s before, to 1.5 km/s after the passage over Great Whale River. Because there is no evidence for a significant parallel potential drop between the ionosphere and the satellite (i.e. there are no ion beams) we infer that the two regions were coupled at the time of the event. The progagation of the disturbance must therefore reach out to ISEE-1 altitudes.

We can estimate one dimension of the discontinuity from the relative velocity of the satellite footprint and the discontinuity combined with the duration of the event. The average relative velocity between the satellite and the discontinuity in the ionosphere was approximately 2.4 km/s which, multiplied by the duration of the strong turbulence of 80 s, gives a width of about 200 km in the ionosphere and 700 km at the position of the satellite.

The discontinuity moved almost transversely to the magnetic field direction. This can be seen by considering the timing of the event from the footprint of the field line from ISEE-1 to Fort Churchill. The arrival of the event at Fort Churchill agrees to within about 1 minute with the expected arrival determined from the event at ISEE-1. The time difference corresponds to about 150 km distance in the ionosphere and to a "tilt" of the discontinuity from the ionosphere to the

satellite of not more than 2 percent away from the normal to the magnetic field direction.

Because the electric field vector at the satellite cannot be measured, it is not possible to compare the $\overline{E} \times \overline{B}$ velocity with the propagation determined from the ground magnetometers. However, previous studies of the motion of auroral forms and of elect·ic fields have shown that the velocities associated with westward surges are usually larger and often in a different direction than the measured E x B flow (<u>Kelley et al.</u>, 1971, 1975), suggesting that the observed motion may be due to propagation of a wave or progressive triggering of an instability.

By combining the ISEE-1 and NOAA-6 observations, and assuming that the system was relatively unchanged during the ∼15 minutes between the two sets of observations, a model of the potential structure can be determined. The lack of field aligned ion beams show that there was essentially no voltage drop below ISEE-1. The electron observations on the other hand suggest that there was a voltage drop > 10 keV above ISEE-1.

Figure 19 shows the main features of the event deduced from the observations. ISEE-1 flew through the system at an altitude below the region of parallel electric field acceleration. The ISEE-1 ion observations indicate that ion heating was occurring at and below the satellite as indicated by the cross-hatching below the satellite in Figure 19. (A model somewhat similar to Figure 19 has been presented by <u>Winningham et al.</u>, (1984) to explain ion observations from Dynamics Explorer).

Energy Source for the Discontinuity

Energy can be transported into the region of interest via particle kinetic energy and via the Poynting Flux associated with field-aligned currents. Studies of S3-3 data (<u>Mozer et al.</u>, 1980) have shown that the contribution of each of these mechanisms is often approximately equal. Since the event studied herein occurred below the region of parallel field acceleration, it might be expected that a substantial fraction of the incident energy would be particle kinetic energy.

The precipitating electron flux observed by the NOAA-6 satellite early in the event was very intense with a peak flux of 200 erg/cm^{2}s. Unfortunately it was not possible to measure the precipitating electrons on ISEE-1 because the loss cone was only $\sim$14° wide and the electron spectrometer did not observe closer than $\sim$20° to the magnetic field direction. However, we do have an indication of the intensity of the precipitating electron flux from our observation of the fluxes just outside the loss cone. These fluxes were observed at ISEE-1 to be 87 erg cm^{-2} s^{-1} (Figure 21) which, given that the ISEE-1 measurements extended only to 7.1 keV, is in reasonable agreement with the 200 erg cm^{-2} s^{-1} observed going into the atmosphere by NOAA-6.

We also suggest that the accelerating potential was high, when the event was observed by ISEE-1. The electron spectrometer observed the electron spectrum from 0.1 to 7.1 keV and obtained a rather flat spectrum in this range. If we assume a typical plasma sheet temperature of E = 1 keV and an acceleration voltage giving a parallel energy of 6 kV we obtain a cone within which the primary beam is collimated of 22° off the magnetic field direction if the acceleration was taking place immediately above ISEE-1. This means that part of the primary beam would have been observed by the spectrometer when it scanned pitch angles around 20°. If the acceleration was taking place further above the satellite the mirror effect would have broadened the beam and it would have been observed over a larger angular range. We therefore find that the accelerating voltage must have been above $\sim$7 kV and indeed the shape of the spectrum of trapped electrons is in agreement with an accelerating voltage of $\sim$10 kV.

It is interesting to note that the trapped electron population (Figure 14) has a tendency to be field-aligned until about 2350:00 UT which is in the period where we observe the strong wave turbulence.

The measured upgoing ion flux is of the order of 10^8 cm^{-2} s^{-1} for several minutes during and after the main event. Taking 250 eV as a typical ion energy the ions carry an upgoing energy flux of about 2.5.10^{10} eV cm^{-2} s^{-1} or 0.04 erg cm^{-2} s^{-1}. This flux cannot be directly compared to the energy in the incident

electron beam because the ions transport the energy transferred to them during the period of intense heating, over a much longer period than the heating itself lasts. Based on the period of very high wave intensity in the 5.6 Hz channel, the heating last., about 80 s, but the outflow of hot ions lasts about 15 minutes or 900 s. Even considering these values we conclude that the energy carried by the ions is only a small fraction of the energy carried by the incident electron beam.

According to Gurnett (1974) auroral kilometric radiation (AKR) dissipates 1 to 2% of the energy available in a substorm. In addition, whistler mode waves, auroral hiss, and other wave modes carry energy away from the heating region. Judging from the intensity and bandwidth of these waves compared to the AKR it is likely that they dissipate an amount of energy similar to the auroral kilometric radiation.

It is useful in this event to consider the overall magnetospheric energy budget, and to estimate the total magnetospheric energy dissipation during the substorm in question. An approximate method for estimating the total energy dissipation, U_T, of the magnetosphere has been given by Akasofu (1981):

$$U_T = U_R + U_J + U_A$$

In this equation, U_R is the ring current energy injection rate

$$U_R = 4 \cdot 10^{20} \left(\frac{\partial D_{st}}{\partial t} + \frac{D_{st}}{\tau_R} \right) \frac{erg}{s}$$

U_J is the ionospheric joule heating rate $2.10^{15}.AE$ erg/s, and U_A is the auroral particle precipitation rate $1.10^{15}.AE$ erg/s. Here AE is the auroral electrojet index in nT and τ_R is the ring current particle lifetime.

Lacking high-resolution AE and Dst values for this event, we must make crude estimates of AE and the time variations of Dst. In analogy with the methods of Baker et al. (1981), we estimate Dst between 2230 and 2330 UT to be 17 nT. Based on

the largest negative auroral zone H-component excursions of 700 nT (at Leirvogur and Narssarssuaq) we estimate the average AE to be 500 nT. From this we get

$$U_R = 3.10^{18} \text{ ergs/s}$$
$$U_J = 1.10^{18} \text{ ergs/s}$$
$$U_A = 5.10^{17} \text{ ergs/s}$$

Summing, we estimate the total magnetospheric energy dissipation rate during this substorm event to have been of order $4.5.10^{18}$ erg/s.

Using the energetic particle intensities observed at geostationary orbit (Figure 8) and using a reasonable estimate of the volume occupied by these particles (see Baker et al. 1981 for details) we compute that some 5.10^{17} erg/s of energy appears in the form of > 30 keV electrons and ions. For a dissipation period of ~1/2 hour, a total of > 10^{21} ergs of energy appears in the energetic particle component and this is 5-10 % of the total energy dissipation inferred from U_T.

If we further examine the energy directly observed by the low-altitude spacecraft, we can assess the inferred low-altitude dissipation within the context of the overall energy budget of this substorm. A peak precipitating energy flux of 200 erg cm^{-2} s^{-1} in the NOAA-6 electrons was measured. If we assume this flux to have been characteristic of $1°$ in invariant latitude and 1 hour of local time, we get an area of precipitation equal to $1.5.10^{15}$ cm^2. Thus, the peak electron precipitation corresponds to

$$1.5.10^{15} \text{ } cm^2 . 200 \text{ erg } cm^{-2} \text{ } s^{-1} = 3.10^{17} \text{ erg/s.}$$

This compares favorably with the estimated particle precipitation energy rate (U_A) of 5.10^{17} erg/s based upon AE measurements.

We conclude that the precipitating electron fluxes as detected by NOAA-6 could have driven essentially all of the local plasma processes associated with the westward travelling surge detected in ISEE-1 and ground-based measurements. Overall, however, the downflowing electrons, the upflowing ions, the AKR dissipation, and the other ionospheric dissipation features

were only a fraction of the total substorm energy available. The ultimate energy source for all of the processes observed here was undoubtedly solar wind energy extracted by the magnetosphere, stored in the tail region, and dissipated by global substorm processes.

Wave Particle Processes

The intense precipitating electron flux observed by the NOAA-6 satellite early in the event had an energy flux of $\sim$80 erg cm^{-2} s^{-1} averaged over 1° latitude with a peak in the energy spectrum at >10 keV. If we take 10 keV as a typical energy then 80 erg cm^{-2} s^{-1} corresponds to a flux of 5.10^9 electrons cm^{-2} s^{-1}. Such a flux will drive the magnetosphere unstable to electrostatic ion cyclotron (EIC) waves down to very low altitudes according to Kindel and Kennel (1971) and it would certainly drive it unstable at altitudes similar to those of ISEE-1. The discontinuity (current sheet or filament) was thus unstable to EIC waves at the time it was observed by NOAA-6.

Although the electron flux at ISEE-1 can not be determined with sufficient accuracy to determine if it is adequate to drive the magnetosphere unstable to electrostatic ion cyclotron waves, the observations show extremely high wave intensities at all frequencies which provides evidence that the magnetosphere must have been unstable at the ISEE-1 position. Electrostatic waves account for a large part of the wave activity, and electrostatic waves are strongly damped by either Landau damping or cyclotron damping when they propagate away from their generation region.

The conic distributions of the upflowing ions show that they have experienced mainly transverse heating and therefore the responsible waves have to be polarized with their electric vectors nearly transverse to the magnetic field. This heating could then be caused by either electrostatic ion cyclotron waves or lower hybrid waves.

The very high wave intensity 10^{-4} V^2 m^{-2} Hz^{-1} at 5.6 Hz results in very fast heating of ions. As shown in the Appendix the characteristic time for change of the distribution function

f is of the order of 1 second and therefore the ions can be heated to the observed energies in a few seconds.

The data in Figure 11 suggest that the ions were heated mainly transversely to the magnetic field except perhaps at 2349:37 and 2350:29 UT where the source cone for the 0.22 keV ions were partially filled. This filling may have been caused by a small parallel electric field at or below the satellite, but the total potential drop in this electric field region must be well below 200 Volts to preserve the conical distributions still seen. Based on the angular widths of the conics we can estimate that the ions at this time came from a region ~4000 km below the satellite, and this region could not have had any parallel potential drops as large as 200 V. Parallel electric fields in this region would also systematically shift the distribution of the higher energy ions and we see no evidence for such an effect in these distributions either.

The development of the pitch angles of the conic ions (Figure 11 and Table 3) show that the ions arrive at ISEE-1 from deeper and deeper below the satellite. A relatively straightforward interpretation of these results is obtained if one assumes that this is a temporal rather than a spatial effect. That is: the "mirror" point or the altitude where the ions have been heated moves down as time progresses. The data supporting this inference are shown in Figure 20. To construct this figure, we have taken the pitch angles at half maximum flux (Table 3) and computed the corresponding upper and lower mirror altitudes which are indicated by the vertical bars. In doing this we have assumed that the gradient of the magnetic field is radial, which is a very good approximation in a dipole field. The slanted line in the top of the figure shows the distance of ISEE-1 from the center of the Earth in Earth radii. One sees from the figure that the mirror points of the hydrogen ions move down quickly and reach below one half Earth radius altitude in less than 4 minutes. The mirror points for oxygen ions move down much more slowly and reach down to a comparable altitude in 10 to 15 minutes. This is qualitatively in agreement with the lower velocity of oxygen ions than protons of the same energy, if one assumes that the time behavior of the observed ions is caused by their varying transit time from different altitudes after a nearly instantaneous heating at the time

of the passage of the discontinuity. This picture is also qualitatively in agreement with the gross variation of ion energies throughout the event in the sense that lower energy ions of both species are observed later in the event.

For 10 minutes previous to the onset of the event there were no ions above background (2. to 3.10^4 cm^{-2} s^{-1} sr^{-1} keV^{-1} except about 10^5 cm^{-2} s^{-1} sr^{-1} keV^{-1} O^+ ions at pitch angles between 160° and 180°. This means that there are very few ions present above 137 eV, which is the lower half-maximum limit of the pass band for the 0.2 keV channel. It is likely that the ions which were heated at the discontinuity were present as cold ions in the magnetosphere around the satellite before the arrival of the discontinuity. Oxygen ions with 0.2 keV energy have a thermal velocity of 50 km/s, and ions with that velocity cannot move very far during the time it takes the satellite to pass the discontinuity, especially not if they have a pitch angle around 90° to 135°. There are only small transverse E-fields present before the event so it seems that there is no way a hot plasma could have been moved to the vicinity of the satellite. Therefore we have to assume that the ions are heated in situ and that they are present as cold ions before the event.

The cold ion population at the position of the satellite, when the discontinuity was encountered, seems to have been 80% to 90% O^+ if one assumes that both O^+ and H^+ are heated to the extent that the ion mass spectrometer obtains a representative sample of the ion population. This estimate is obtained in the following way: The O^+ flux is larger than the H^+ flux by a factor of two to three. The velocity of O^+ ions is lower than the velocity of H^+ ions at the same energy by a factor of 4 because of the mass ratio. Combining these two facts yields a density of hot O^+ that is an order of magnitude higher than the density of H^+.

This estimate assumes that the O^+ and H^+ have the same temperature. As discussed above, the H^+ temperature immediately after the occurrence of the discontinuity is rather close to the O^+ temperature, and therefore the estimate is probably rather good at this time. However, after the outflow of ions has started we probably cannot expect any close connection between the temperatures of the two species because of their

velocity difference. Since the outflowing ions initially observed on ISEE-1 came from the altitude range ~3000 to ~10000 km we infer that this region of the magnetosphere was very rich in oxygen at the time of this event.

Particle acceleration.

The particle acceleration or particle heating during the event are of two kinds. The observations at NOAA-6 shows that there must be a field aligned acceleration of electrons toward the Earth. Some of the primary electrons are scattered by the atmosphere and reflected by the Earth's magnetic field. These electrons are not able to penetrate the electric field region on their return and thus become trapped between an electric mirror above and a magnetic mirror below. It is this trapped radiation that is seen in the electron phase space densities after the passage of the discontinuity. The electron phase space densities have been integrated to obtain the particle densities shown in Figure 15. The hot plasma densitiy jumps to 24 cm^{-3} at the passage of the discontinuity and then level off at ~10 cm^{-3}. This is a rather high density at an altitude above 10000 km and shows that all the ambient plasma at ISEE-1 takes part in the plasma processes.

The energy flux carried by electrons in the energy range 0.1 to 7.0 keV has been integrated for up and downgoing electrons separately. The observed up and downgoing fluxes are equal except for statistical fluctuations as shown in Figure 21. This supports the view that the field aligned fluxes observed just after the passage of the discontinuity are carried by trapped electrons.

Before the discontinuity the up and downgoing energy fluxes is of the order of 0.1 erg cm^{-2} s^{-1}. At the discontinuity they jump to ~80 erg cm^{-2} s^{-1} and during the next three minutes it slowly falls to 1.0 erg cm^{-2} s^{-1}.

The primary electron beam and/or the up and downgoing trapped electron fluxes drive the magnetosphere unstable to plasma waves at and below ISEE-1 and probably also to some distance above the satellite, but this can not be demonstrated. The

plasma waves heat the ions at and below the satellite and, as discussed previously, they are probably EIC waves since they heat the ions transverse to the magnetic field at a very fast rate. (They could also be LHR waves which are also polarized transverse to the field, but the very fast heating rate indicate a resonance effect and this points to EIC waves).

The transversely heated ions are pushed up the field line away from the Earth by the μ·grad B force. This force gives a 250 eV proton an initial acceleration of ~ 4.3 km/s^2 and an 250 eV oxygen ion an acceleration of 270 m/s^2 and quickly pushes this transversely heated plasma toward the electric field region above. Here the ions are accelerated by the electric field in the electric potential jump in this case to an energy in the range 10-15 keV. On the outer part of the field line we have a field aligned beam of ions with an energy in this range directed toward the equator.

We know from magnetograms from Halley Bay (Alan Rodger, personal communication, 1983) that the substorm occurred in both hemispheres. Unless there is a potential difference between the northern and southern auroral oval, we have a field aligned beam of ions also from the southern hemisphere directed towards the equator. These two ion beams penetrate the ambient plasma in the equatorial region (or each other) and plasma interaction causes strong electrostatic ion cyclotron instability (Michelsen, 1976; Michelsen et al., 1976) that tends to isotropize the plasma. Since the interaction length is long it is reasonable to assume that the resulting plasma will be a nearly isotropic plasma with a temperature of the order of 10 to 15 keV.

This plasma is mainly heated transverse to the magnetic field and is partially trapped between the two electric field regions below and will only be partially observable at low altitudes.

The upgoing ions will tend to neutralize the space charge region near the equator, but because of the sluggishness of the ions they will arrive in the equatorial region several minutes after the onset of the event and this means that the end of the event probably is caused by electron drain from the space charge region rather than by neutralization by upflowing ions.

An alternative explanation of the sudden flux increase at geostationary orbit may be a sudden temperature change in the ambient plasma caused by plasma instability. The cause of the plasma instability could be the previously mentioned ion beams penetrating the ambient plasma in the equatorial region or interpenetrating ion beams. On the satellite 1976-059 we observe a sudden increase above instrument threshold by a factor of 10^5. As an example let us assume a final temperature of 15 keV and that our instrument measures energies above 150 keV. We then find that a change in temperature by a factor of 2 from 7.5 to 15 keV will change the observed flux by 5 orders of magnitude. We therefore suggest that a sudden onset of plasma heating caused by strong energetic ion beams should be considered as a possible alternative explanation to plasma sheet thinning to explain sudden flux increases at geostationary orbit. It could also be the mechanism causing the injection boundary of McIlwain (1974). In this paper McIlwain stresses that the ATS-5 data strongly suggests the existence of in situ heating of the plasma at the injection boundary and Mauk and Meng (1983) argue that their energy dispersion observations on the SCATHA satellite are quite different from the dispersion predictions obtained from the convection model. We plan to continue to examine these possibilities in future work.

Finally we must stress the role of ion dynamics in the development of a substorm. The ISEE-1 observations show that the heating processes in the magnetosphere are strongly anisotropic. We note especially the transverse heating of ions at intermediate altitudes along the field lines. The mirror force will move these ions up along the field lines with velocities that can not exceed the thermal velocities of the ions and the lower energies may take several tens of minutes to reach the equatorial plane. This is comparable to the duration of the recovery phase and suggests that ion dynamics plays an important role in the recovery process and is an important factor in determining the duration of the recovery phase. The substorm can not be expected to end until a stage much closer to equilibrium is reached than the one we have observed in this westward travelling surge.

APPENDIX

The electrostatic waves interact with ions in the ambient medium, and if the waves are polarized transversely to the magnetic field they will mainly affect the transverse velocity of the ions. The interaction is customarily treated with the Fokker-Planck equation, which for this case can be written as a diffusion equation (Sturrock, 1966). The resulting diffusion equation is

$$\frac{Df}{Dt} = \frac{\partial}{\partial w_\perp}\left(D_{\perp\perp}\frac{\partial f}{\partial w_\perp}\right)$$

where f is the distribution function and $w_\perp$ the transverse energy of the ions.

The transverse diffusion constant is in cgs units

$$D_{\perp\perp} \simeq \frac{w_\perp e^2}{8m} P_\gamma^E$$

where P_γ^E is the power spectral density of the electrostatic waves. The power spectral density in the first 80 s of the discontinuity at 5.6 Hz is 10^{-4} V^2 m^{-2} Hz^{-1} which gives a diffusion constant of

$$D_{\perp\perp} \simeq 1.2 \, w_\perp \frac{(keV)^2}{s}$$

for protons. The local diffusion equation has the form

$$\frac{\partial f}{\partial t} = \Gamma \frac{\partial}{\partial w_\perp}\left(w_\perp \frac{\partial f}{\partial w_\perp}\right)$$

with $\Gamma w_\perp = D_{\perp\perp}$. This equation leads asymptotically to a Maxwellian distribution

$$f(w_\perp, t) \simeq \frac{1}{\Gamma t} \exp\left(-\frac{w_\perp}{\Gamma t}\right)$$

The characteristic time scale for changes in f is (Dusenbery and Lyons, 1981)

$$T_f \simeq \frac{1}{D_{\perp\perp}}$$

and this time scale should be larger than the period of the waves $T_\omega = 1/\omega_{EIC}$. The above value of $D_{\perp\perp}$ gives a characteristic time for the change of f of the order of one second and

$$T_f \simeq 1 \gg T_\omega = \frac{1}{\omega_{EIC}} \simeq \frac{1}{18}$$

which assures us that quasi-linear theory is valid even in this case where the characteristic time for changing the distribution function is of the order of one second.

REFERENCES:

Akasofu, S.-I.,
    Polar and Magnetospheric Substorms,
    D. Reidel/Dordrecht-Holland, p. 37ff., 1968.
Akasofu, S.-I.,
    Energy Coupling Between the Solar Wind and the Magnetosphere,
    Space Sci. Rev., 28, 121-190, 1981.
Akasofu, S.-I., R. H. Eather and J. N. Bradbury,
    The Absence of the Hydrogen Emission (H_β) in the
    Westward Travelling Surge,
    Planet. Space Sci., 17, 1409-1412, 1969.
Akasofu, S.-I., D. S. Kimball, and C.-I. Meng,
    Dynamics of the Aurora. II. Westward
    Travelling Surges,
    J. Atm. Terr. Phys., 27, 173-187, 1965.
Akasofu, S.-I., and C.-I. Meng,
    The Abnormally Early Appearance of Active Auroras,
    J. Atm. Terr. Phys., 29, 601-602, 1967a.
Akasofu, S.-I., and C.-I. Meng,
    The Abnormally Early Appearance of the Eastward
    Motion of Auroras in the Evening,
    J. Atm. Terr. Phys., 29, 1029-1031, 1967b.
Akasofu, S.-I., and C.-I. Meng,
    Intense Negative Bays Inside the Auroral Zone I.
    The Evening Sector,
    J. Atm. Terr. Phys., 29, 965-973, 1967c.
Akasofu, S.-I., and C.-I. Meng,
    Auroral Activity in the Evening Sector,
    J. Atm. Terr. Phys., 29, 1015-1018, 1967d.
Akasofu, S.-I., C.-I. Meng, and D. S. Kimball,
    Dynamics of the Aurora. IV. Polar Magnetic
    Substorms and Westward Travelling Surges,
    J. Atm. Terr. Phys., 28, 489-496, 1966.
Baker, D. N., T. A. Fritz, B. Wilken, P. R. Higbie, S. M. Kaye,
    M. G. Kivelson, T. E. Moore, W. Studemann, A. J. Masley,
    P. H. Smith, and A. L. Vampola,

Observation and Modeling of Energetic Particles at Synchronous
Orbit on July 29, 1977,
J. Geophys. Res., 87, 5917-5932, 1982.

Baker, D. N., E. W. Hones, Jr., P. R. Higbie, R. D. Belian,
and P. Stauning,
Global Properties of the Magnetosphere During a Substorm
Growth Phase: A Case Study,
J. Geophys. Res., 86, 8941-8956, 1981.

Baumjohann, W., R. J. Pellinen, H. J. Opgenoort, and E. Nielsen,
Joint Two-Dimensional Observations of Ground Magnetic and
Ionospheric Electric Fields Associated with Auroral
Zone Currents: Current Systems Associated with Local
Auroral Break-Ups,
Planet. Space Sci., 29, 431-447, 1981.

Dusenbery, P. B., and L. R. Lyons,
Generation of Ion-Conic Distribution by Upgoing
Ionospheric Electrons,
J. Geophys. Res., 86, 7627-7638, 1981.

Evans, D. S.,
Precipitating Electron Fluxes Formed by a Magnetic
Field Aligned Potential Difference,
J. Geophys. Res., 79, 2853-2858, 1974.

Fairfield, D. H., R. P. Lepping, E. W. Hones, Jr., S. J. Bame,
and J. R. Asbridge,
Simultaneous Measurements of Magnetotail Dynamics by
IMP Spacecraft,
J. Geophys. Res., 86, 1396-1414, 1981.

Gurnett, D. A.,
The Earth as a Radio Source: Terrestrial Kilometric Radiation,
J. Geophys. Res., 79, 4227-4238, 1974.

Gurnett, D. A., F. L. Scarf, R. W. Fredricks, and E. J. Smith,
The ISEE-1 and ISEE-2 Plasma Wave Investigation,
IEEE Trans. on Geoscience Electronics, GE-16, 225-230, 1978.

Hill, V. J., and D. S. Evans,
The TIROS-N Total Energy Flux Instrument: A Monitor
of Energy Input to the Atmosphere by Auroral Particles,
EOS, 61, 1060, 1980.

Inhester, B., W. Baumjohann, R. A. Greenwald, and E. Nielsen,
Joint Two-Dimensional Observations of Ground Magnetic
and Ionospheric Electric Fields Associated with Auroral
Zone Currents,

J. Geophys., 49, 155-162, 1981.

Kelley, M. C., G. Haerendel, H. Kappler, F. S. Mozer, and
U. V. Fahleson,
Electric Field Measurements in a Major Magnetospheric
Substorm,
J. Geophys. Res., 80, 3181-3195, 1975.

Kelley, M. C., F. S. Mozer, and U. V. Fahleson,
Electric Fields in the Nighttime and Daytime Auroral Zone,
J. Geophys. Res., 76, 6054-6066, 1971.

Kindel, J. M., and C. F. Kennel,
Topside Current Instabilities,
J. Geophys. Res., 76, 3055-3078, 1971.

Kisabeth, J. L., and G. Rostoker,
The Expansive Phase of Magnetospheric Substorms,
1. Development of the Auroral Electrojets and Auroral Arc
Configuration during a Substorm,
J. Geophys. Res., 79, 972-984, 1974.

Lyons, L. R., and D. S. Evans,
An Association Between Discrete Aurora and Energetic
Particle Boundaries,
J. Geophys. Res., 89, 2395-2400, 1984.

Marklund, G., W. Baumjohann, and I. Sandahl,
Rocket and Ground-Based Study of an Auroral Breakup Event,
Planet. Space Sci., 31, 207-220, 1983.

McIlwain, C. E.,
Substorm Injection Boundaries,
in Magnetospheric Physics, B. M. McCormac, Ed., p. 143-154,
D. Reidel Publishing Company, Dordrecht-Holland, 1974.

Mauk, B. H., and C. I. Meng,
Dynamical Injections as the Source of Near Geostationary
Quiet Time Particle Spatial Boundaries,
J. Geophys. Res., 88, 10011-10024, 1983.

Mende, S. B., R. D. Sharp, E. G. Shelley, G. Haerendel and E. W. Hones,
Coordinated Observations of the Magnetosphere: The Development
of a Substorm,
J. Geophys. Res., 77, 4682-4699, 1972.

Meng, C.-I., A. L. Snyder, Jr., and H. W. Kroehl,
Observations of Auroral Westward Travelling Surges
and Electron Precipitations,
J. Geophys. Res., 83, 575-585, 1978.

Michelsen, P.,

Stability Limits of the Ion Beam Excited Electrostatic
Ion Cyclotron Instability,
Phys. Fluids, 19, 337-339, 1976.

Michelsen, P., H. L. Pecseli, J. Juhl Rasmussen and N. Sato,
Unstable Electrostatic Ion Cyclotron Waves Excited by
an Ion Beam,
Phys. Fluids., 19, 453, 1976.

Mozer, F. S., C. A. Cattell, M. K. Hudson, R. L. Lysak,
M. Temerin, and R. B. Torbert,
Satellite Measurements and Theories of Low Altitude Auroral
Particle Acceleration,
Space Sci. Rev., 27, 155-213, 1980.

Mozer, F. S., R. B. Torbert, U. V. Fahleson, C.-G. Falthammar,
A. Gonfalone, and A. Pedersen,
Measurements of Quasi-Static and Low-Frequency Electric
Fields with Spherical Probes on the ISEE-1 Spacecraft,
IEEE Trans. Geoscience Electronics, GE-16, 258-261, 1978.

Ogilvie, K. W., J. D. Scudder, and H. Doong,
The Electron Spectrometer Experiment on ISEE-1,
IEEE Trans. Geoscience Electronics, GE-16, 261-265, 1978.

Opgenoorth, H. J., R. J. Pellinen, W. Baumjohann, E. Nielsen,
G. Marklund, and L. Eliasson,
Three-Dimensional Current Flow and Particle Precipitation
in a Westward Travelling Surge (Observed During the Barium-
GEOS Rocket Experiment),
J. Geophys. Res., 88, 3138-3152, 1983.

Opgenoorth, H. J., R. J. Pellinen, H. Maurer, F. Kueppers,
W. J. Heikkila, K. U. Kaila, and P. Tanskanen,
Ground-Based Observations of an Onset of Localized Field-
Aligned Currents Durint Auroral Breakup Around Magnetic
Midnight,
J. Geophys., 48, 101-115, 1980.

Reme, H., and J. M. Bosqued,
Rocket observation of Electron Precipitation in a
Westward-Travelling Surge,
J. Geophys. Res., 78, 5553-5558, 1973.

Rostoker, G., S.-I. Akasofu, J. Foster, R. A. Greenwald, Y. Kamide,
K. Kawasaki, A. T. Y. Lui, R. L. McPherron, and C. T. Russell,
Magnetospheric Substorms - Definition and Signatures,
J. Geophys. Res., 85, 1663-1668, 1980.

Rostoker, G., and J. L. Kisabeth,

Response of the Polar Electrojets in the Evening Sector
to Polar Magnetic Substorms,
J. Geophys. Res., 78, 5559-5571, 1973.

Russell, C. 1.,
The ISEE 1 and 2 Fluxgate Magnetometers,
IEEE Trans. Geoscience Electronics, GE-16, 239-242, 1978.

Sandahl, I., L. Eliasson, and R. Lundin,
Electron Spectra over Discrete Auroras as Measured by the
Substorm-GEOS Rockets,
ESA SP-152, June 1980.

Shelley, E. G., R. D. Sharp, R. G. Johnson, J. Geiss, P. Eberhardt,
H. Balsiger, G. Haerendel, and H. Rosenbauer,
Plasma Composition Experiment on ISEE-A,
IEEE Trans. Geoscience Electronics, GE-16, 266-270, 1978

Sturrock, P. A.,
Stochastic Acceleration,
Phys. Rev., 141, 186-191, 1966.

Tighe, W., and G. Rostoker,
Characteristics of Westward Travelling Surges During
Magnetospheric Substorms,
J. Geophys., 50, 51-67, 1981.

Wiens, R. G., and G. Rostoker,
Characteristics of the Development of the Westward Electrojet
During the Expansive Phase of Magnetospheric Substorms,
J. Geophys. Res., 80, 2109-2128, 1975

Winningham, J. D., J. L. Burch, and R. A. Frahm,
Bands of Ions and Angular V's: A Conjugate Manifestation
of Ionospheric Ion Acceleration,
J. Geophys. Res., 89, 1749-1754, 1984.

FIGURE CAPTIONS

Figure 1

Horizontal component of the Earth's magnetic field from April 20, 1981 2000 UT to April 21, 0200 UT. These magnetograms show the development of the substorm that starts at 2330 UT and the progression of the associated westward travelling surge. The observatories are shown on the map in Figure 2 and the times shown are the starting times of the event.

Figure 2

Map of the Atlantic and Eastern North America showing location of observatories and footprints of fieldlines from the satellites NOAA-6, 1976-059 and ISEE-1 based on a model of the Earth's magnetic field.

Figure 3

Interplanetary magnetic field measured by ISEE-3 on April 20, 1981 from 1800 to 2400 UT. Units are nT.

Figure 4

Examples of electron spectra observed by NOAA-6 showing a distinct peak in the spectrum around 6 keV.

Figure 5

NOAA-6 observations of count rate of field aligned protons in the energy range 30-80 keV, of precipitated energy flux of low energy electrons, and characteristic energy of the precipitated low energy electrons (i.e. The energy at which the electron flux maximized).

Figure 6

NOAA-6 Observations of precipitated and trapped electrons above 30 keV and protons in the range 30 to 80 keV.

Figure 7

Precipitated energy flux as a function of dipole latitude for the NOAA-6 pass April 20, 1981 2327-2353 UT. The energy flux is averaged over 1° latitude intervals and is dominated by low energy electrons. Note the low latitude of the event.

Figure 8

Observations of energetic electrons and ions from the satellite 1976-059 in geostationary orbit at 64° W longitude.

Figure 9

ISEE-1 observations of the Z-component of the Earth's magnetic field (GSE coordinates) and the spin modulated DC electric field in the xy-plane.

Figure 10

ISEE-1 electric field observations on an expanded time scale. The event starts at 2348:30 UT. Note "turbulent" electric fields 23:48:30-2348:45 UT and 2349:00-2349:40 UT caused by strong low frequency electrostatic waves.

Figure 11

Conic beams of ions observed by the ISEE-1 ion-mass-spectrometer. The upper row of frames show the O^+ observations and the lower row the H^+ observations. The H^+ conics ends in the 2353:21 to 2352:13 UT frame whereas the O^+ conics continue for another 10 minutes.

Figure 12

Upper panel shows the parallel phase space density of electrons in the range 0.1 to 7 keV. electrons in the lower part of that panel are moving downward in the direction of the magnetic field vector. Three levels of the natural logarithm of parallel phase space density are contoured in Figure 12a: ln F = -20 (the inner closed contours), ln F = -24 (heavy line), and ln F = -26 (outer light line). Note the Pc4 pulsation in low energy electrons before the event at 2348:30 UT. The lower panel shows the wave observations in the frequency range from 5.6 Hz to 311 kHz. Amplitude is logarithmic and full scale about 100 dB above noise level.

Figure 13

Upper panel shows the parallel phase space density of electrons on an expanded time scale. Down in this panel is again down towards the Earth. In Figure 13a, successive contoured levels of ln F differ by unity. The contours are labelled by -ln F. The discontinuity and the last two Pc4 pulsations before it are clearly shown. In the lower panel is shown the calibrated wave data from the lowest four channels of the filter bank. Saturation in the 5.6 Hz channel is 10^{-4} V^2 m^{-2} Hz^{-1} or 10 mV m^{-1} $Hz^{-1/2}$.

Figure 14

Electron phase space density. There are 9 seconds between frames. The first pair of frames on the left show isotropic electron distribution just before the discontinuity. The other two pairs after the discontinuity show a parallel distribution of electrons. The direction of the magnetic field is to the right in the upper row of frames. The lower row of frames show the parallel phase space density obtained by integrating over transverse velocity. The lower set of dots excludes the loss cone whereas the upper set of dots (heavy) assumes linear interpolation over the loss cone.

Figure 15

Electron density of hot electrons obtained from numerical integration of the phase space density of electrons in the energy range 0.1-7.0 keV.

Figure 16

Wave spectrum over the range 0.1 kHz to 400 kHz from 2330 UT on April 20, 1981 to 0100 UT on April 21.

Figure 17

Calibrated wave data for the period 2348 to 2352 UT. Note the "spiky" nature of the wave amplitude both in the auroral hiss range (0.5 to 31 kHz) and in the auroral kilometric radiation (AKR) at higher frequencies.

Figure 18

Wave spectrum just before and just after the event occurred at ISEE-1. Note the high intensity at the lowest frequencies and the peaks at 200 Hz ($\sim$LHR) and $\sim$50 and $\sim$100 kHz.

Figure 19

Model used to explain the combined observations of the event observed on April 20, 1981 at 2348 UT by ISEE-1.

Figure 20

Altitude of origin of the observed ion conics. The scale on the left shows the distance from the center of the Earth in Earth radii. The slanted dashed line is the distance of ISEE-1. The vertical dashed line show the altitude of origin of the H^+ conics derived from the pitch angle distributions. The vertical full lines show the same for the O^+ ions.

Figure 21

Up and down-going electron energy fluxes derived from the electron phase space density observations. The up and downgoing fluxes are identical when one takes the uncertainty of the observations into consideration.
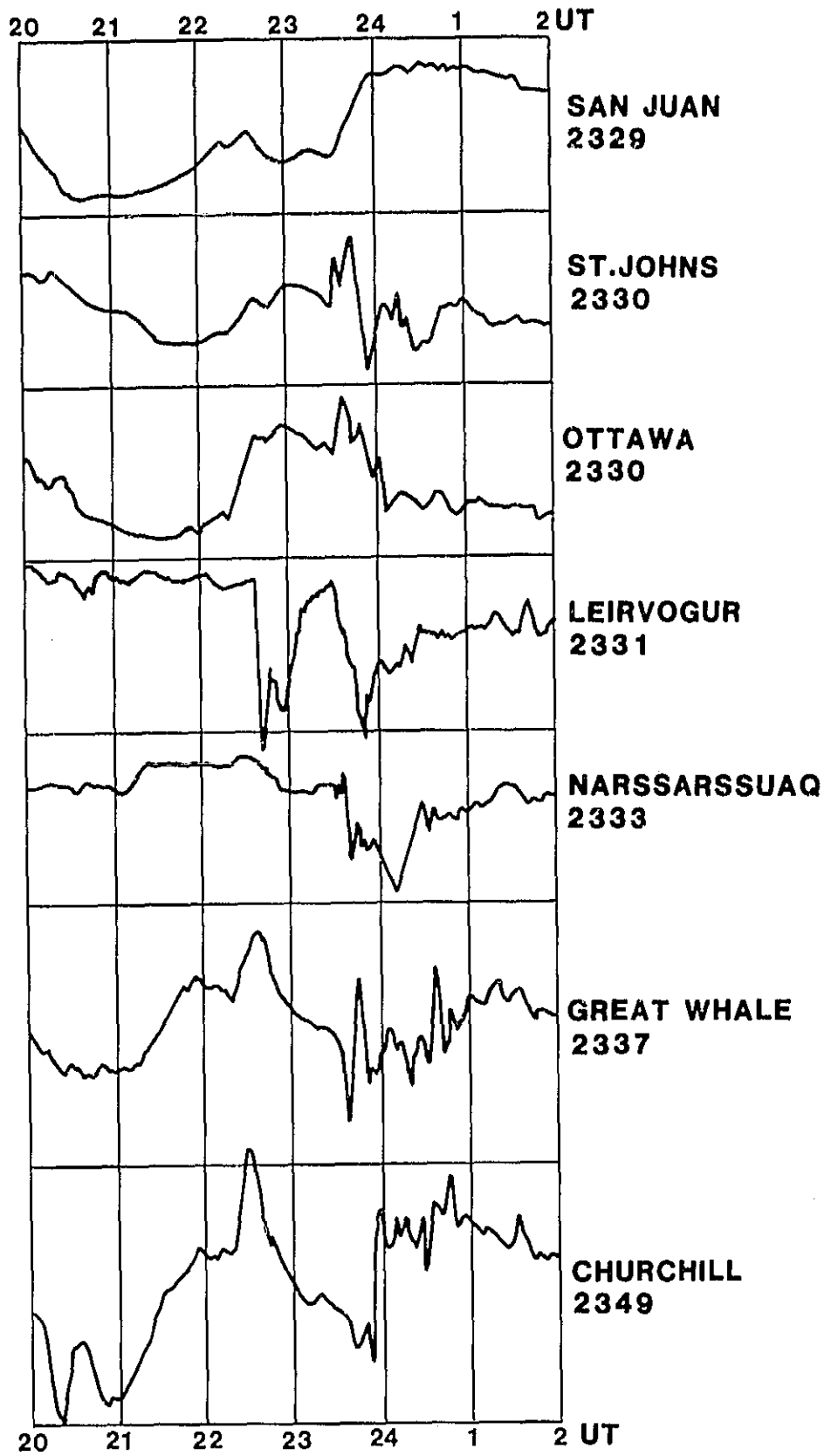
Figure 1
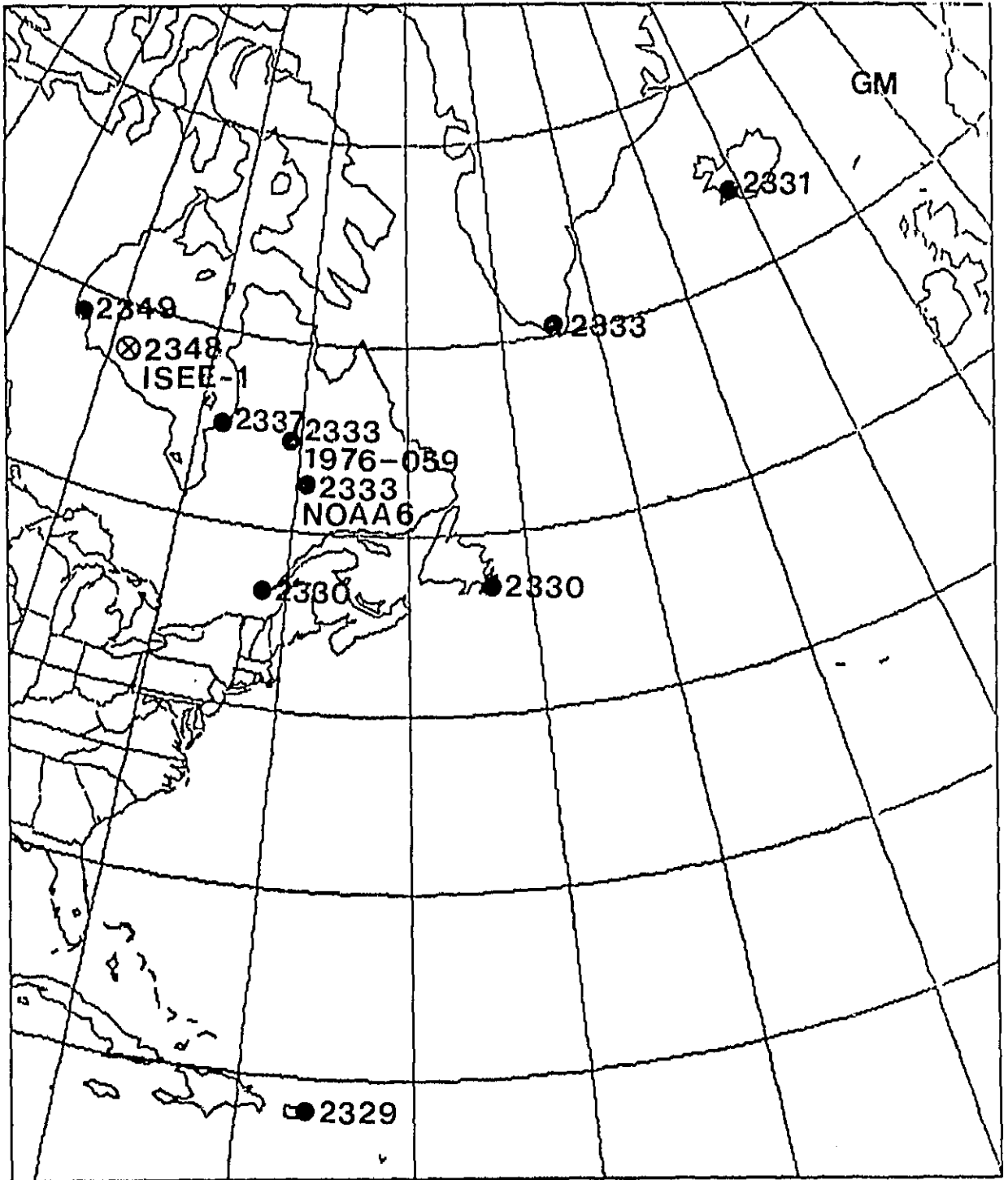
Figure 2

ISEE-3 MAGNETOMETER
1981 DAY 110 I,S COORDS 1 MIN AVGS
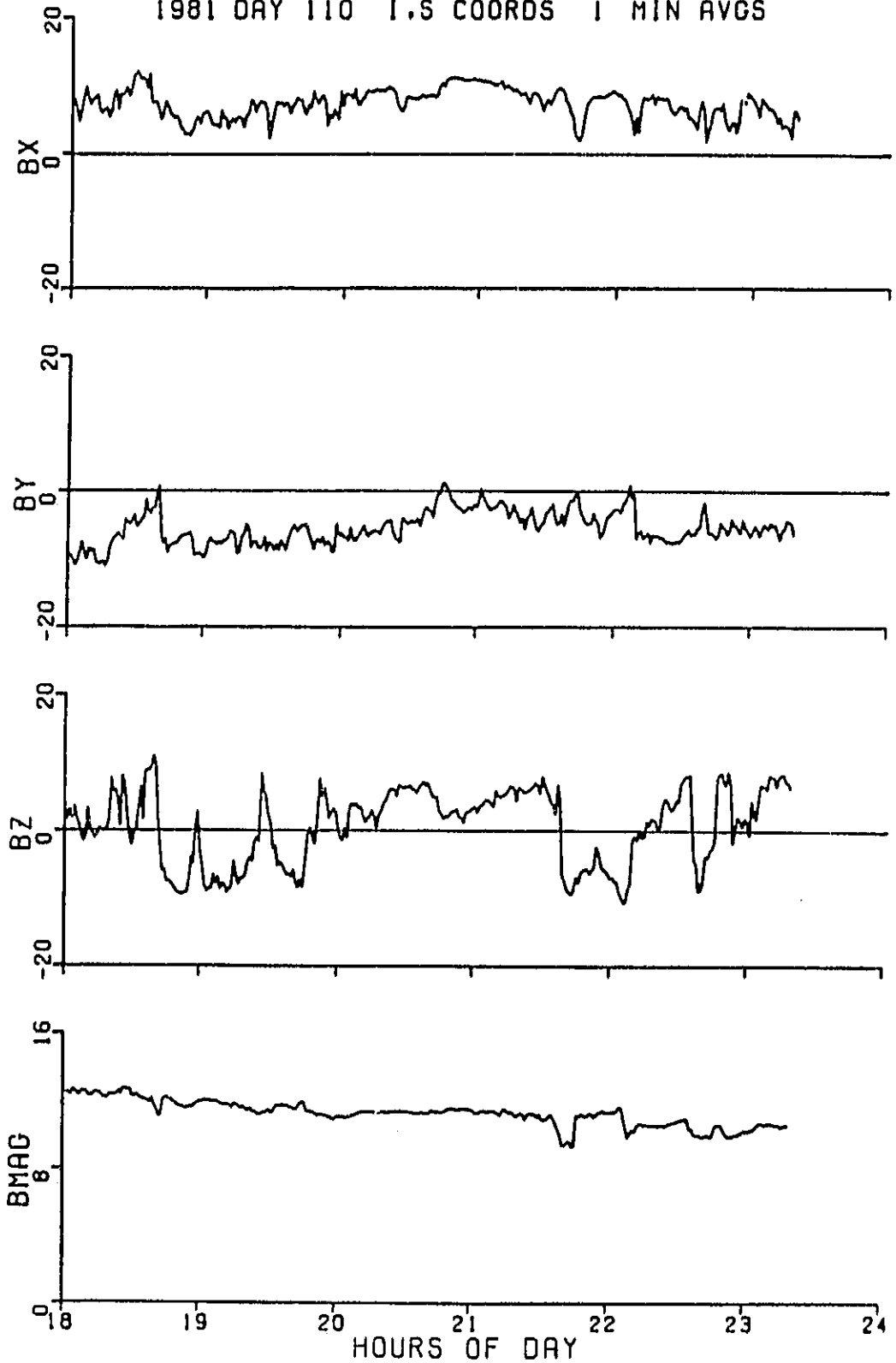
Figure 3

NOAA-6   20 APRIL 1981
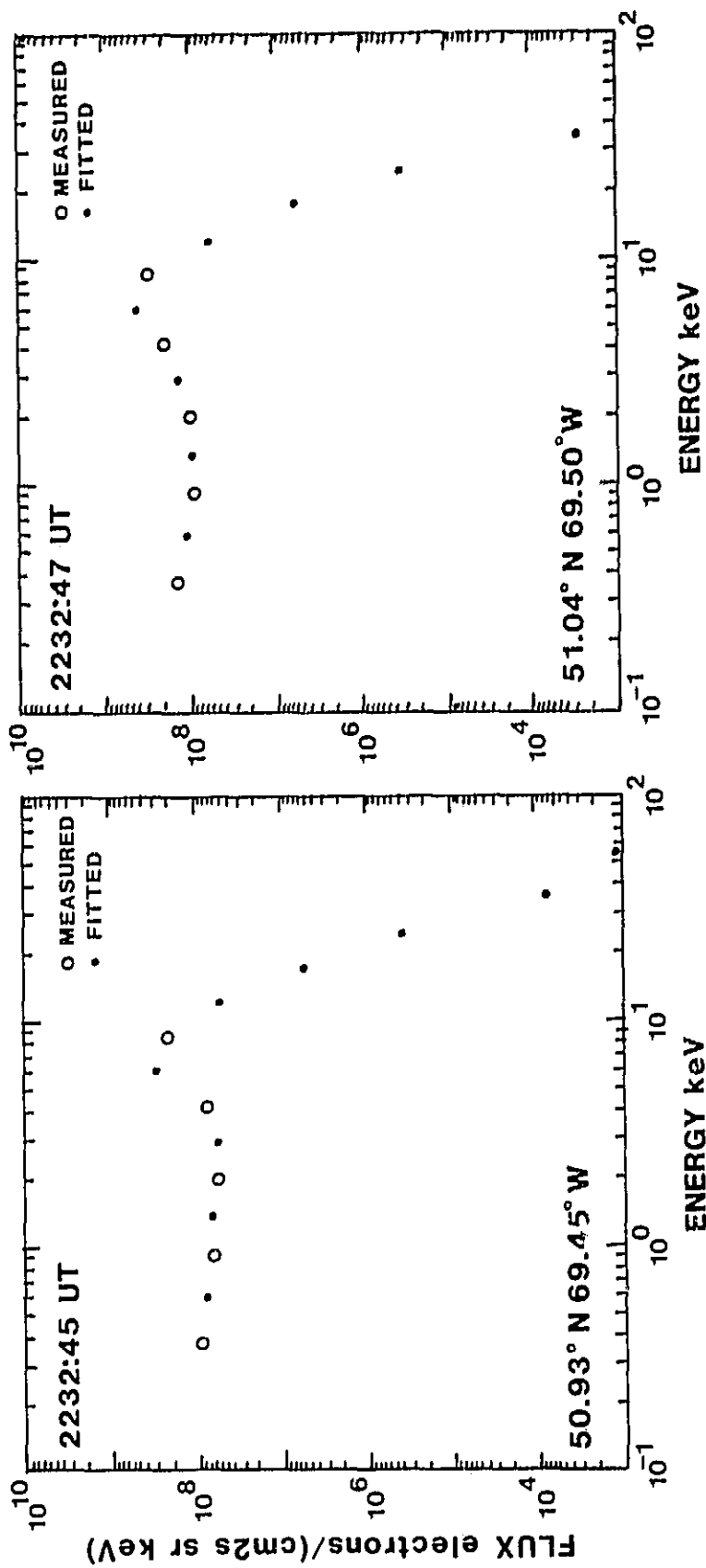
Figure 4
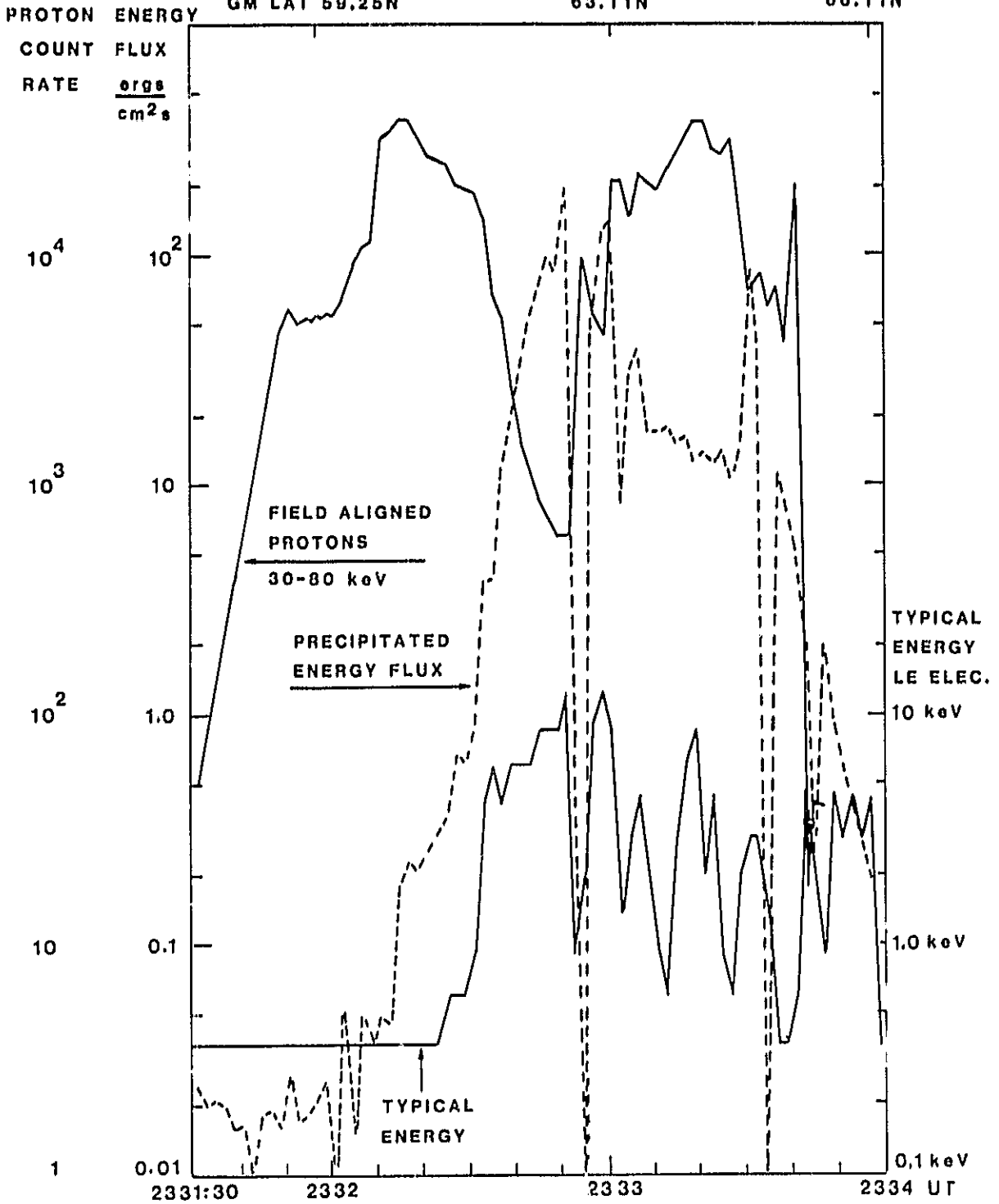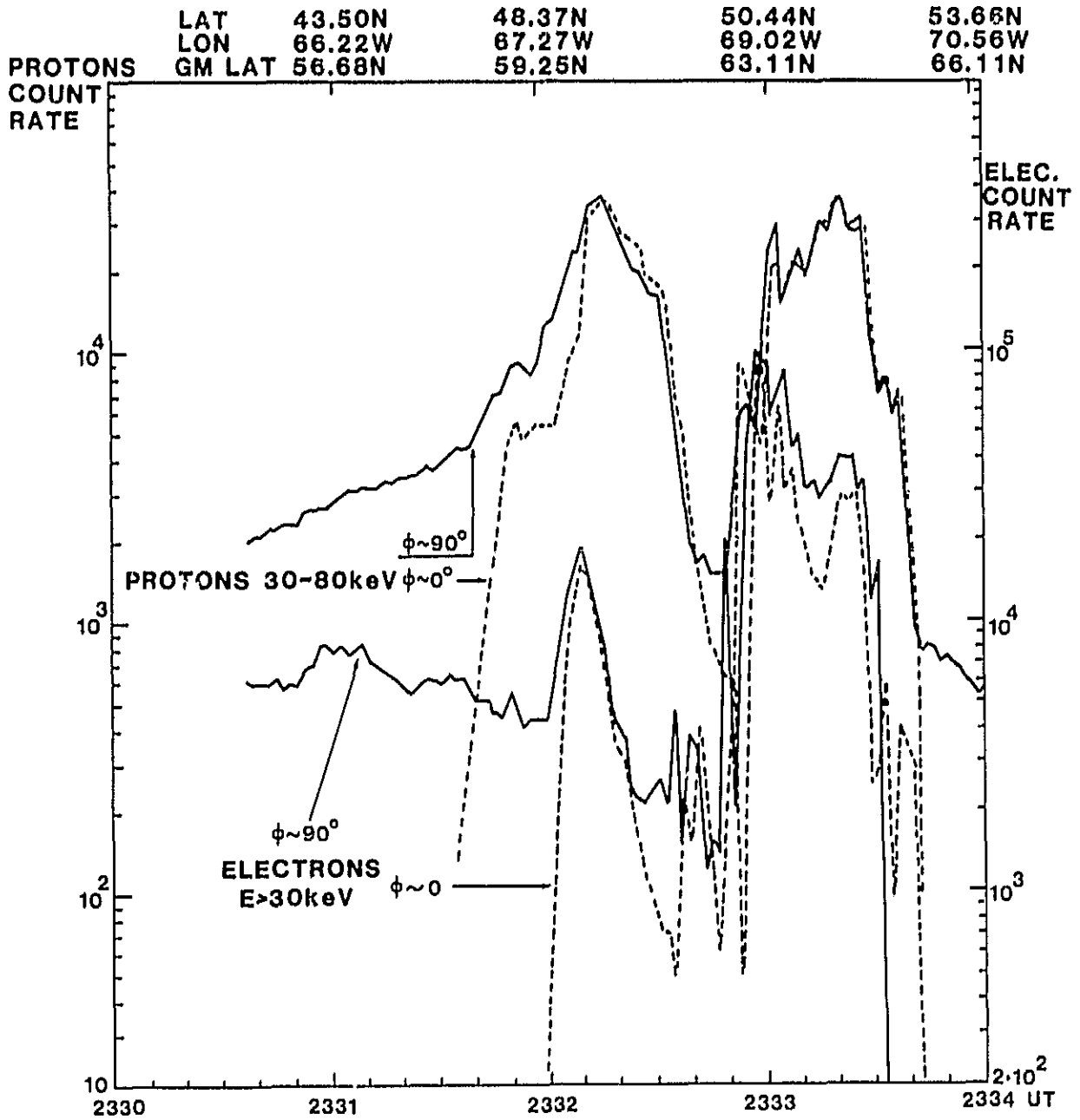
Figure 5

Figure 6

NOAA-6   20 APR.1981   2327 TO 2353 UT
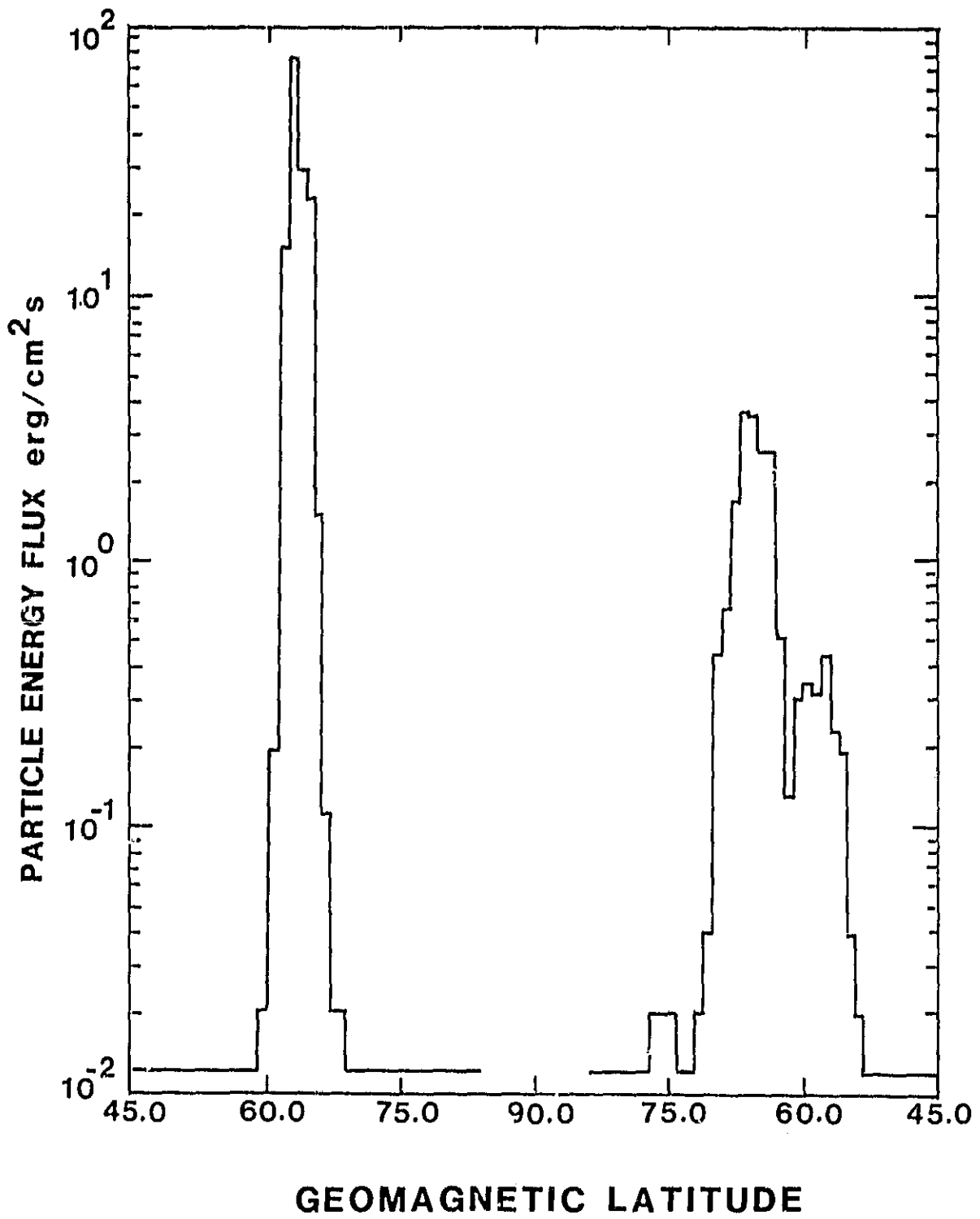
Figure 7
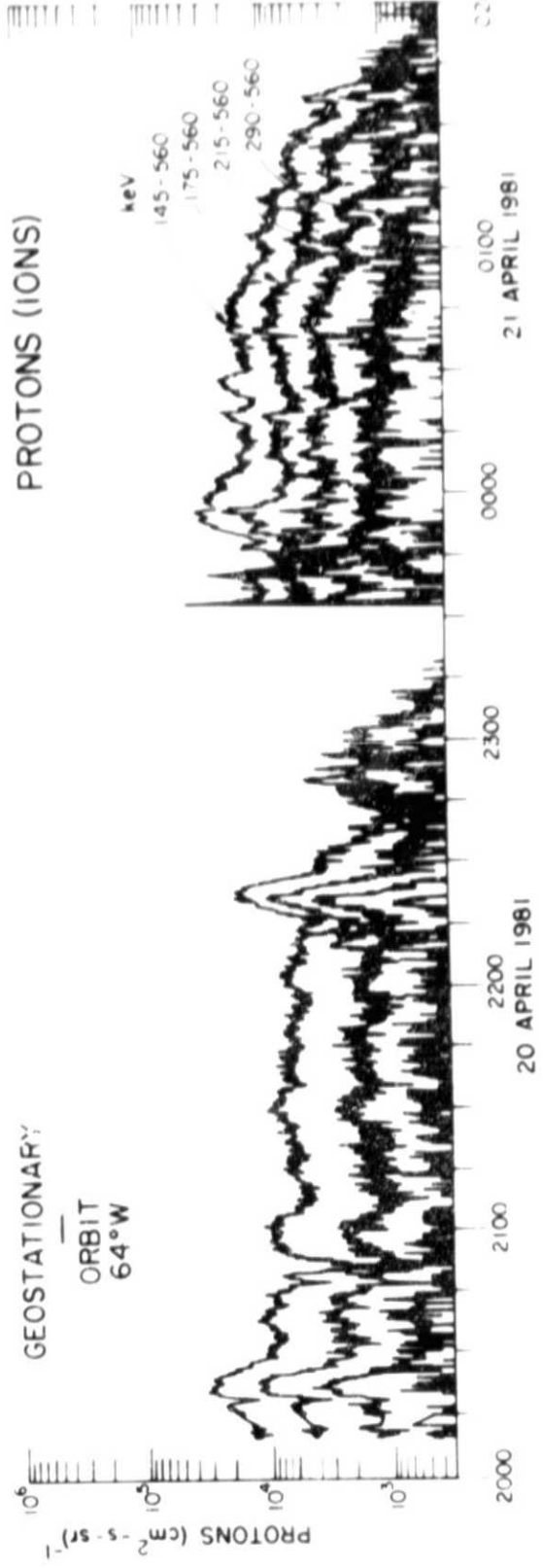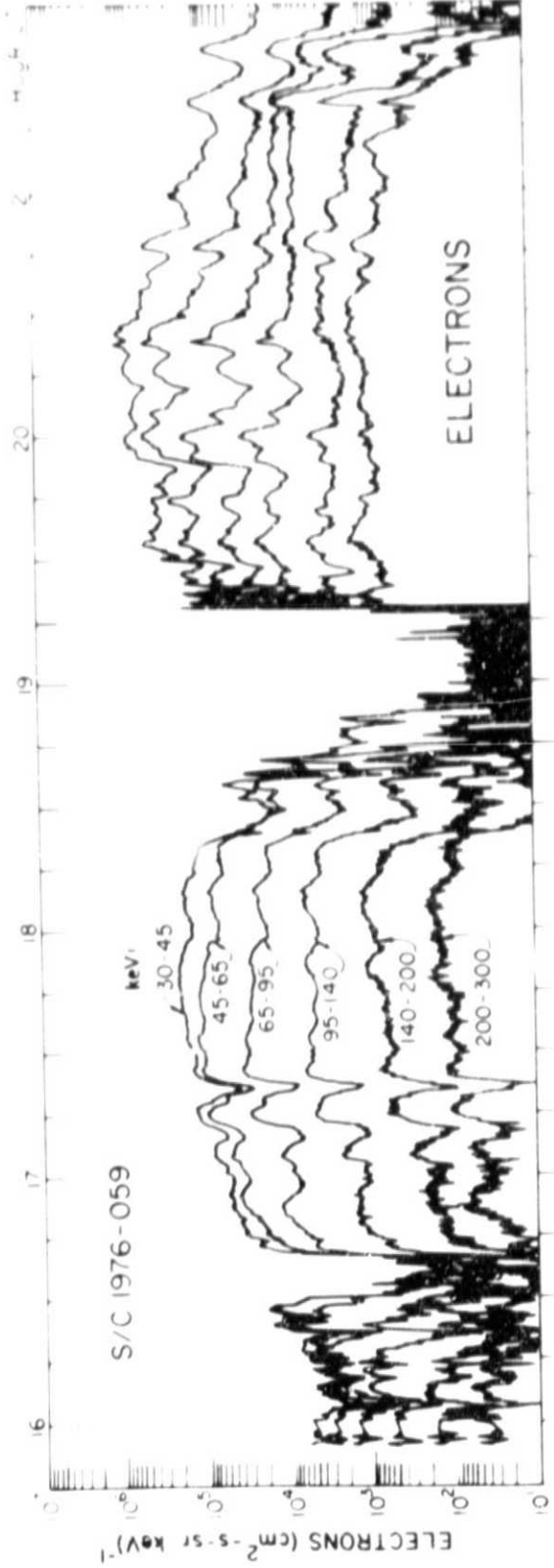
Figure 8
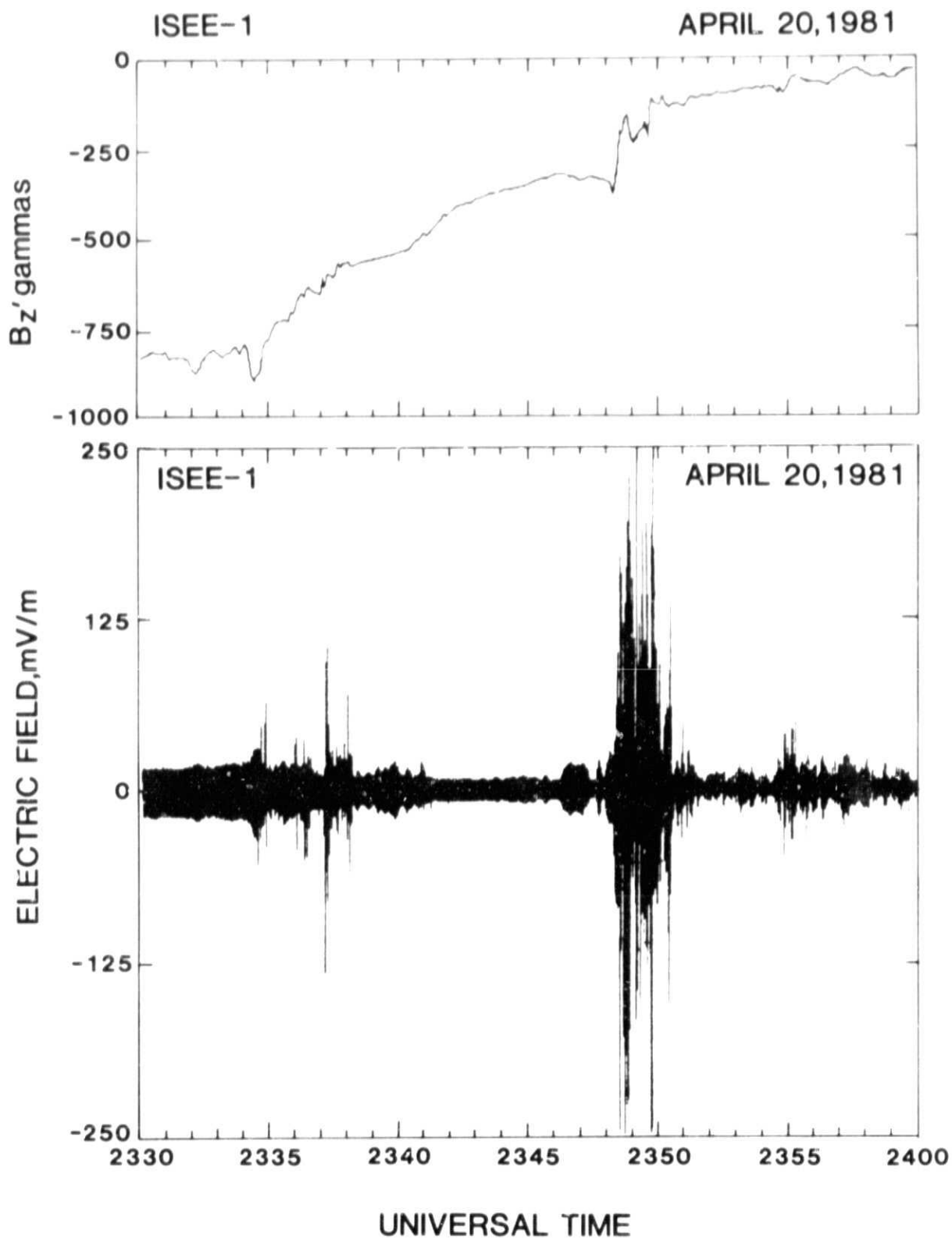
Figure 9
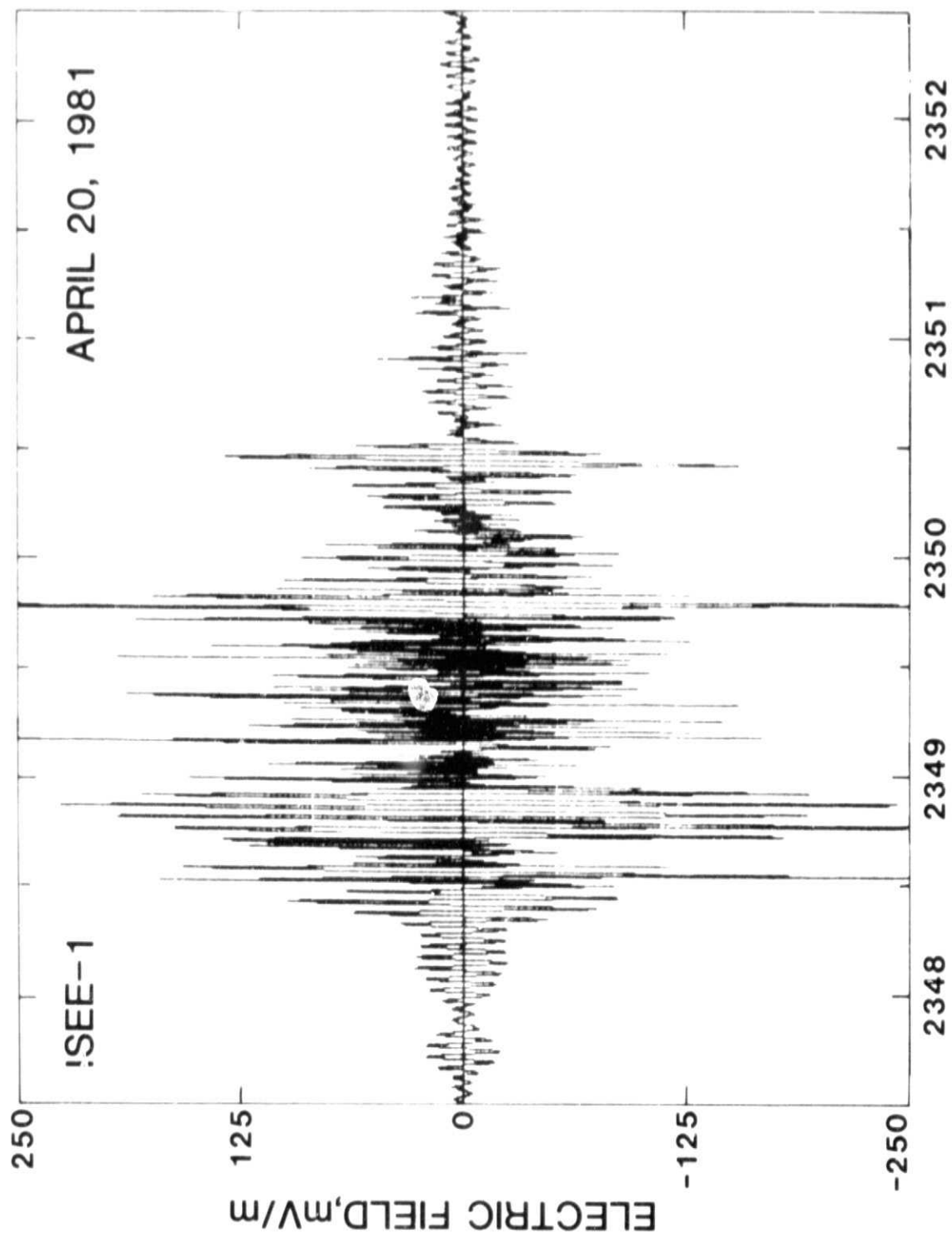
Figure 10

ISEE-1   20 APRIL 1981
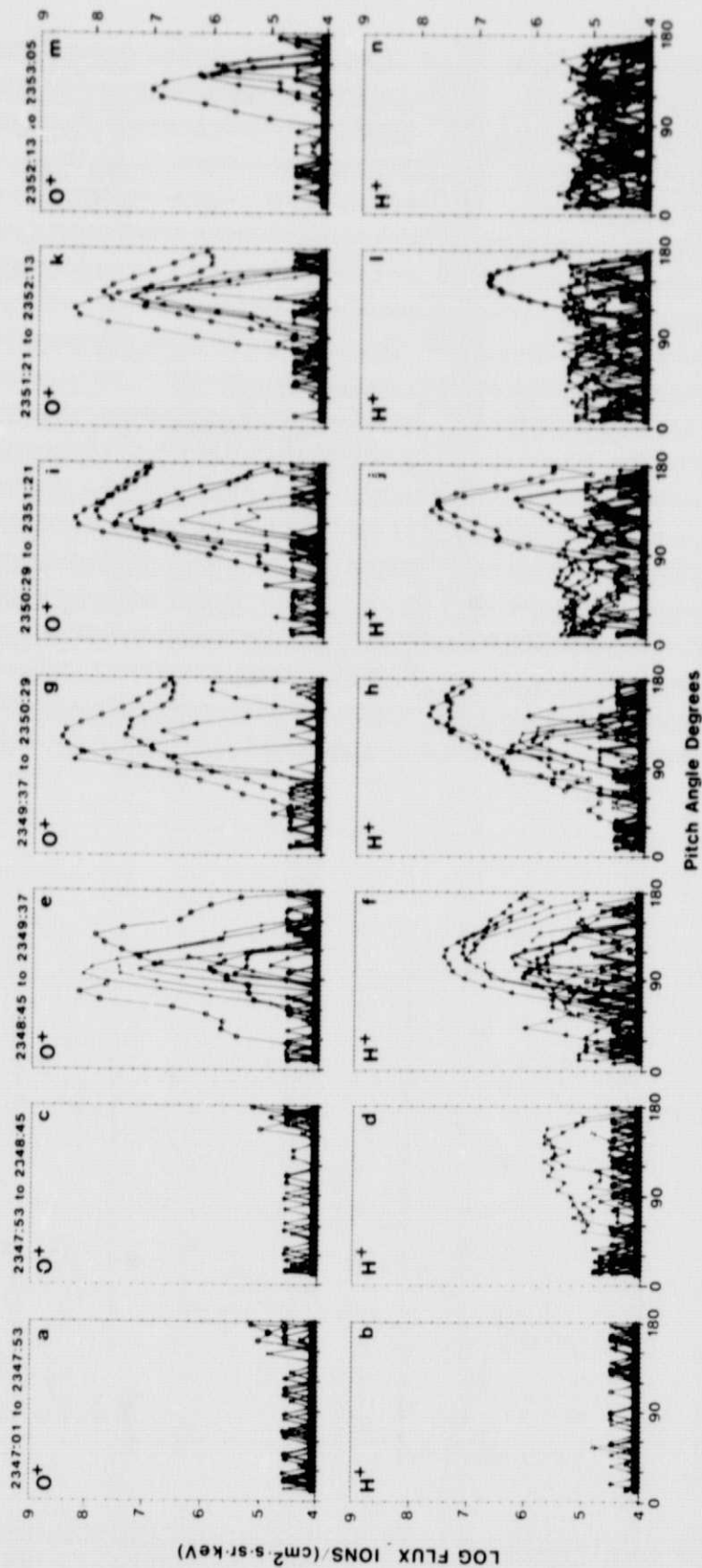
Figure 11
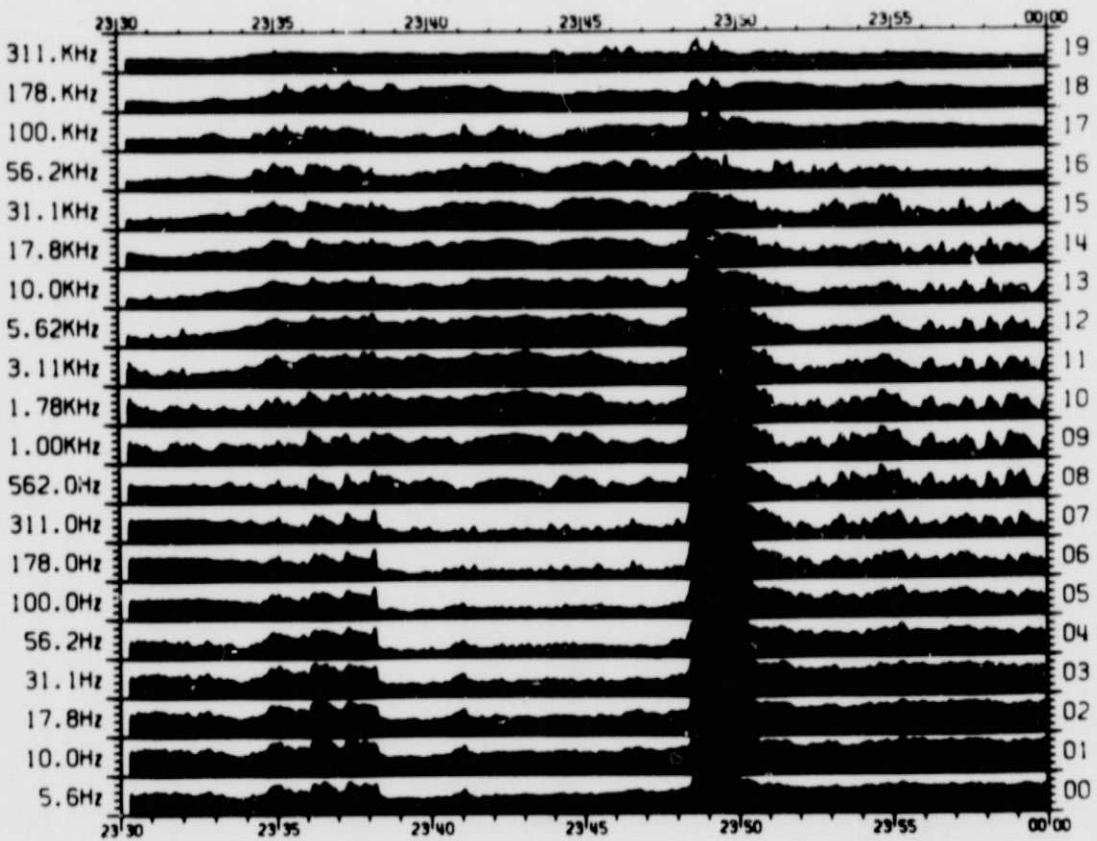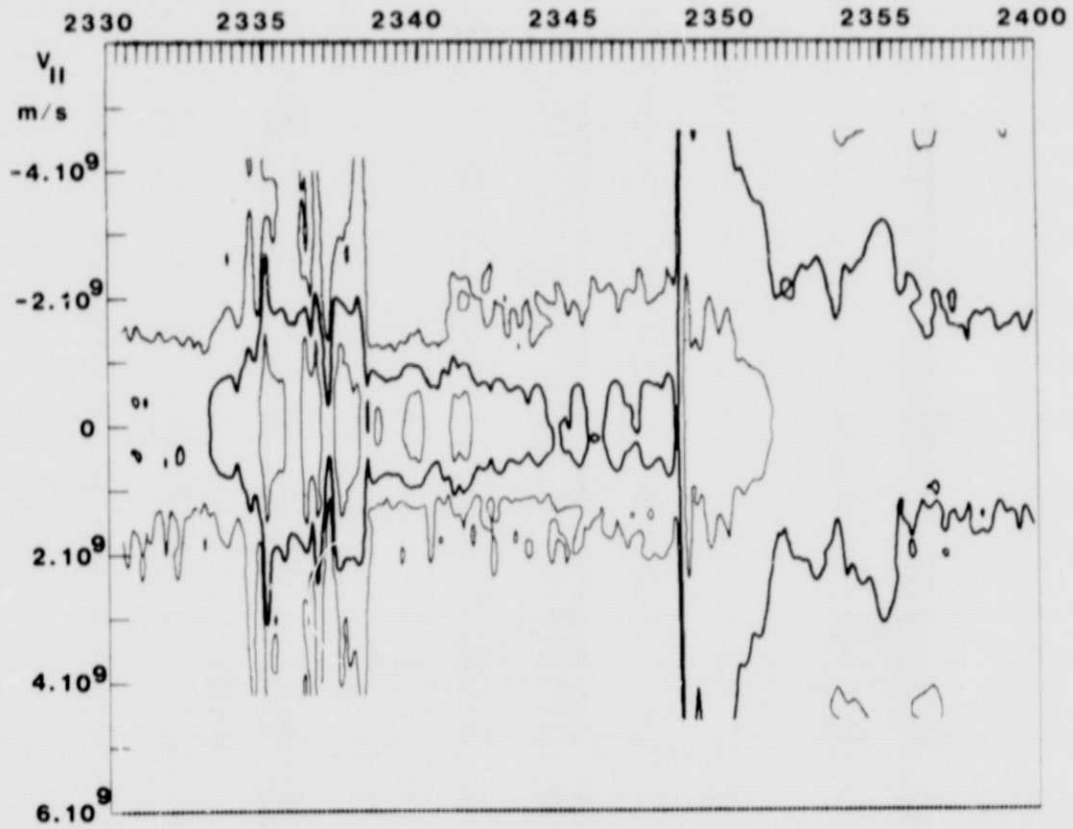
Figure 12
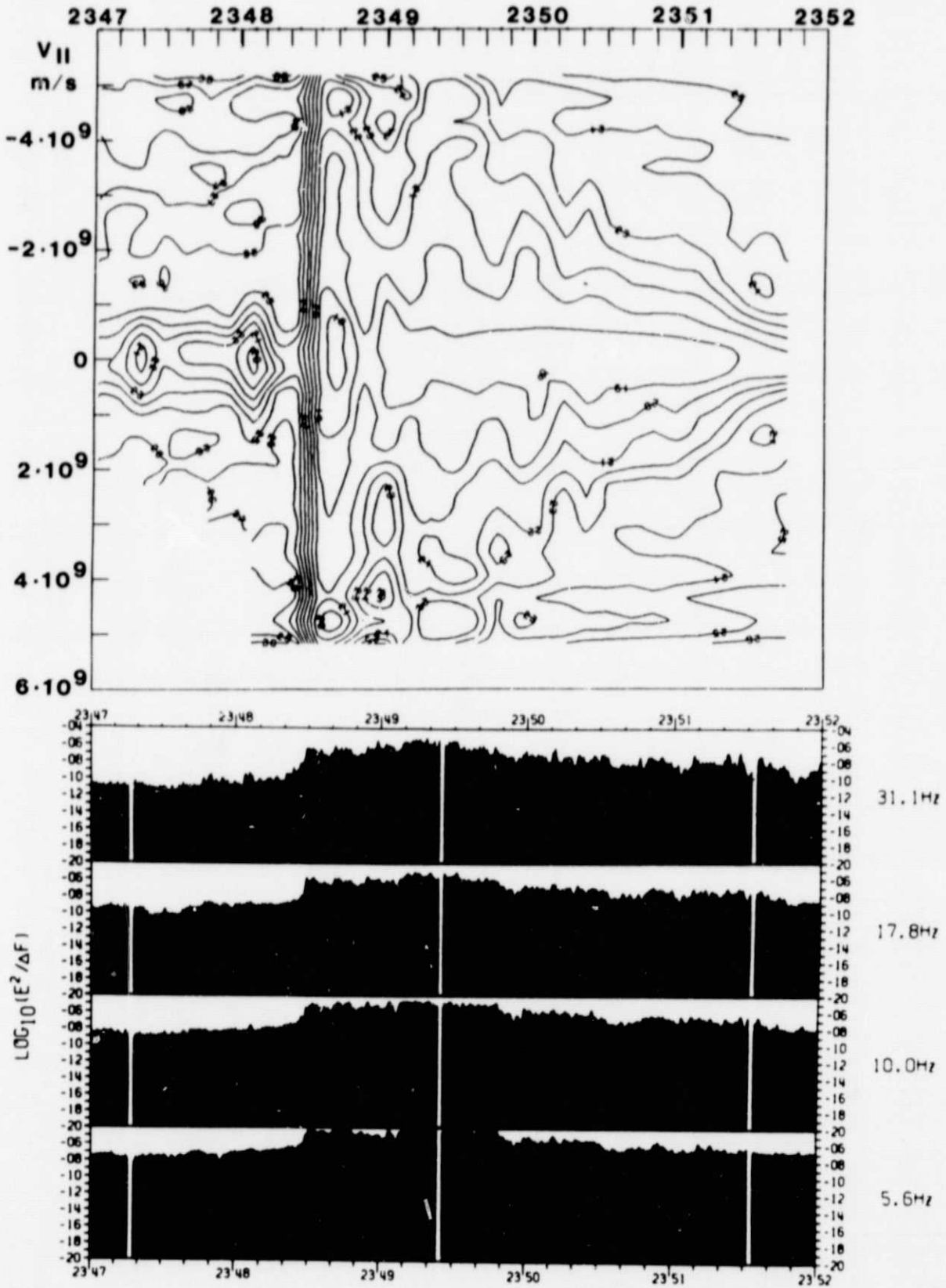
Figure 13

Figure 14

Figure 15

GMT 81 110 23 30   APR 20, 1981

FREQUENCY (HZ)

Figure 16

E**2/ΔF : (VOLT**2)/(METER**2)*(HZ)

Z=5   IPLSFR 800709   RUN 82 075 18
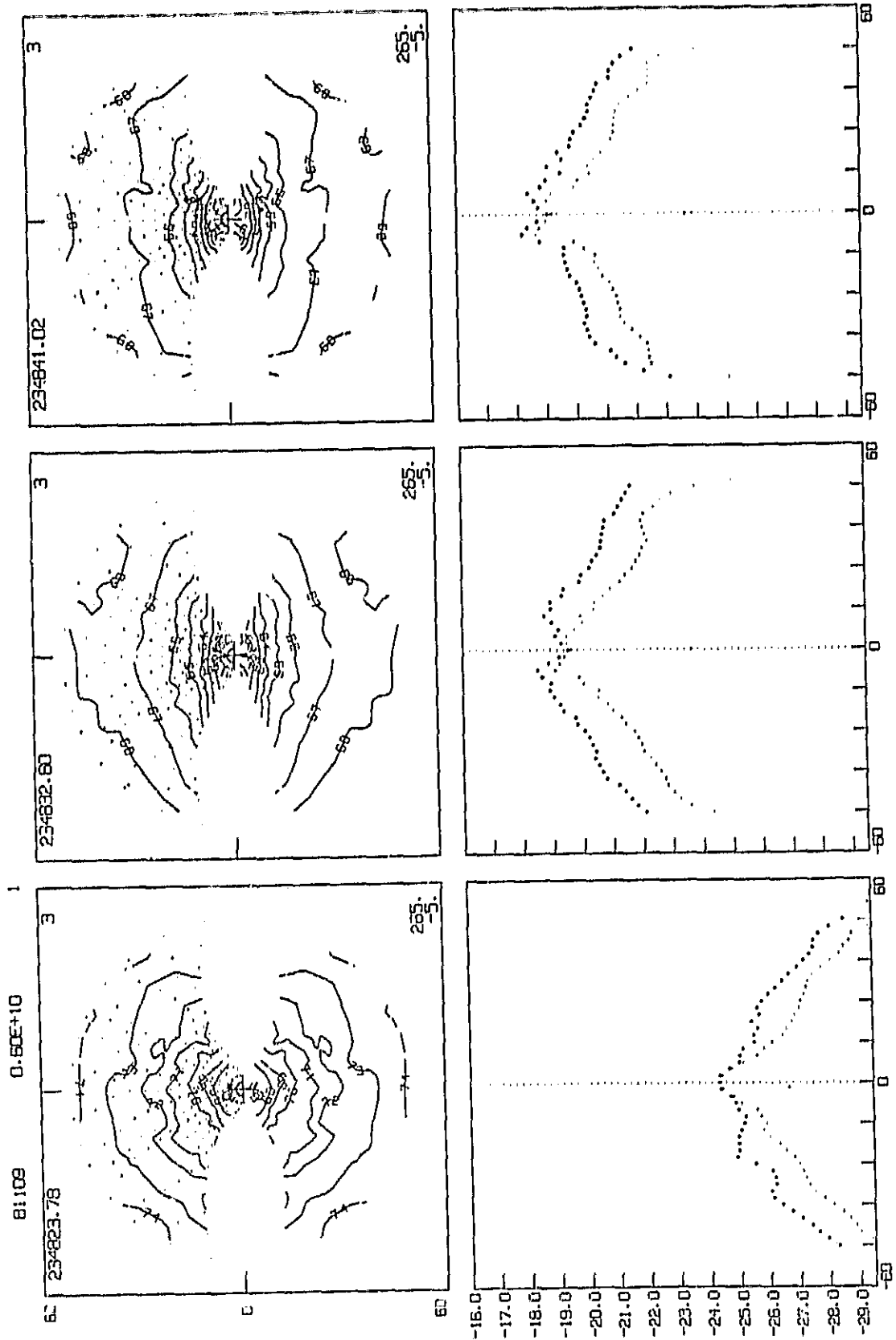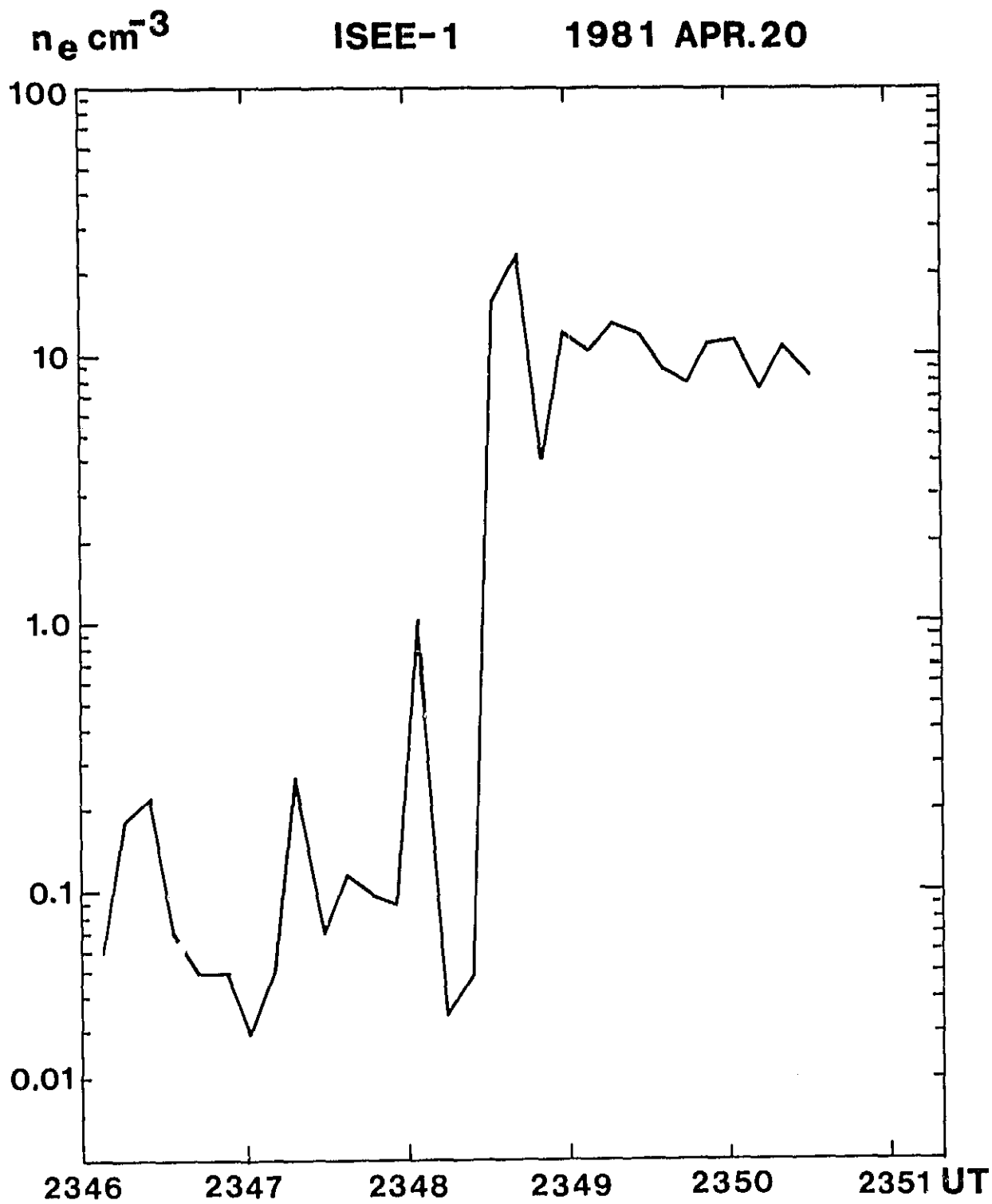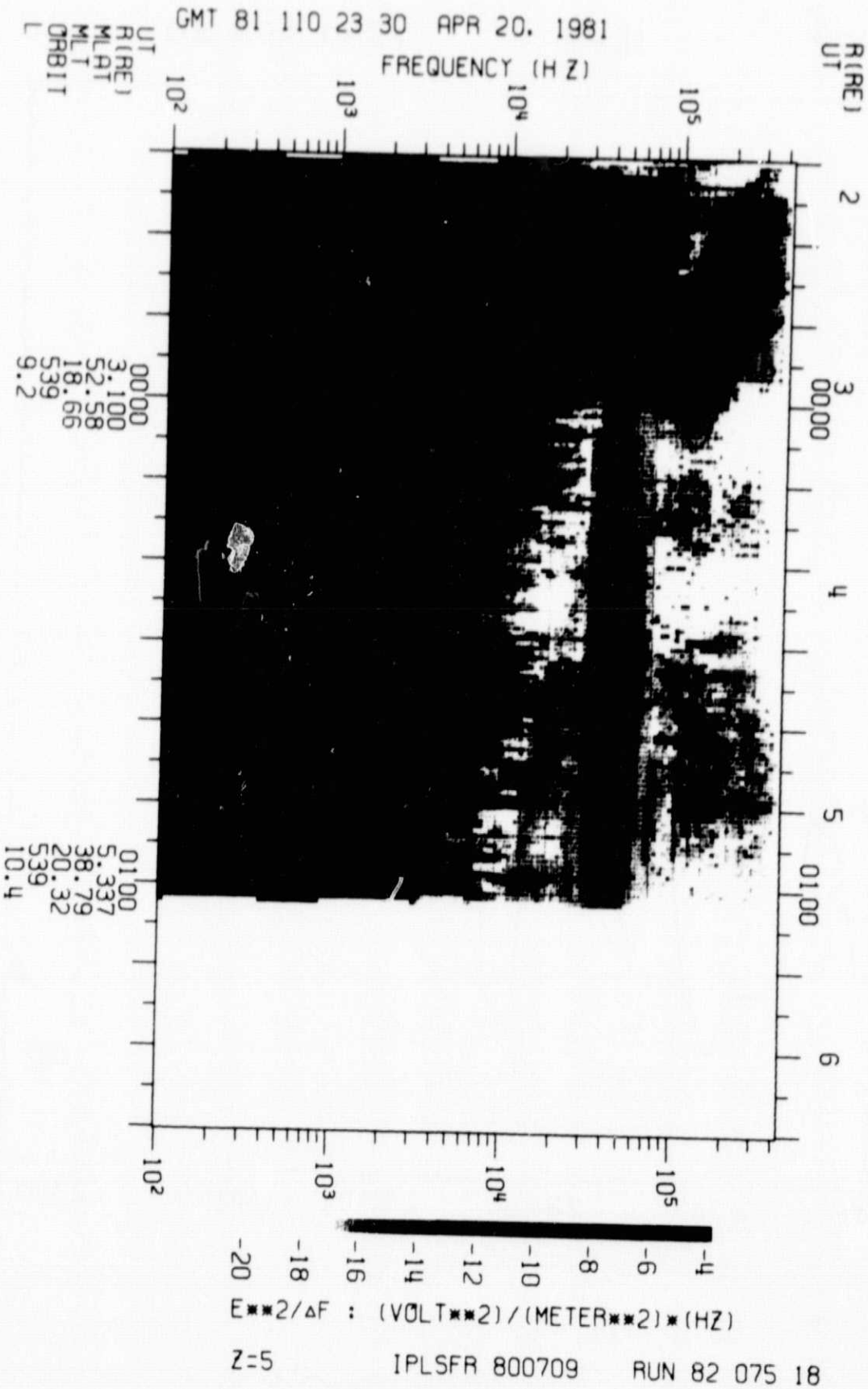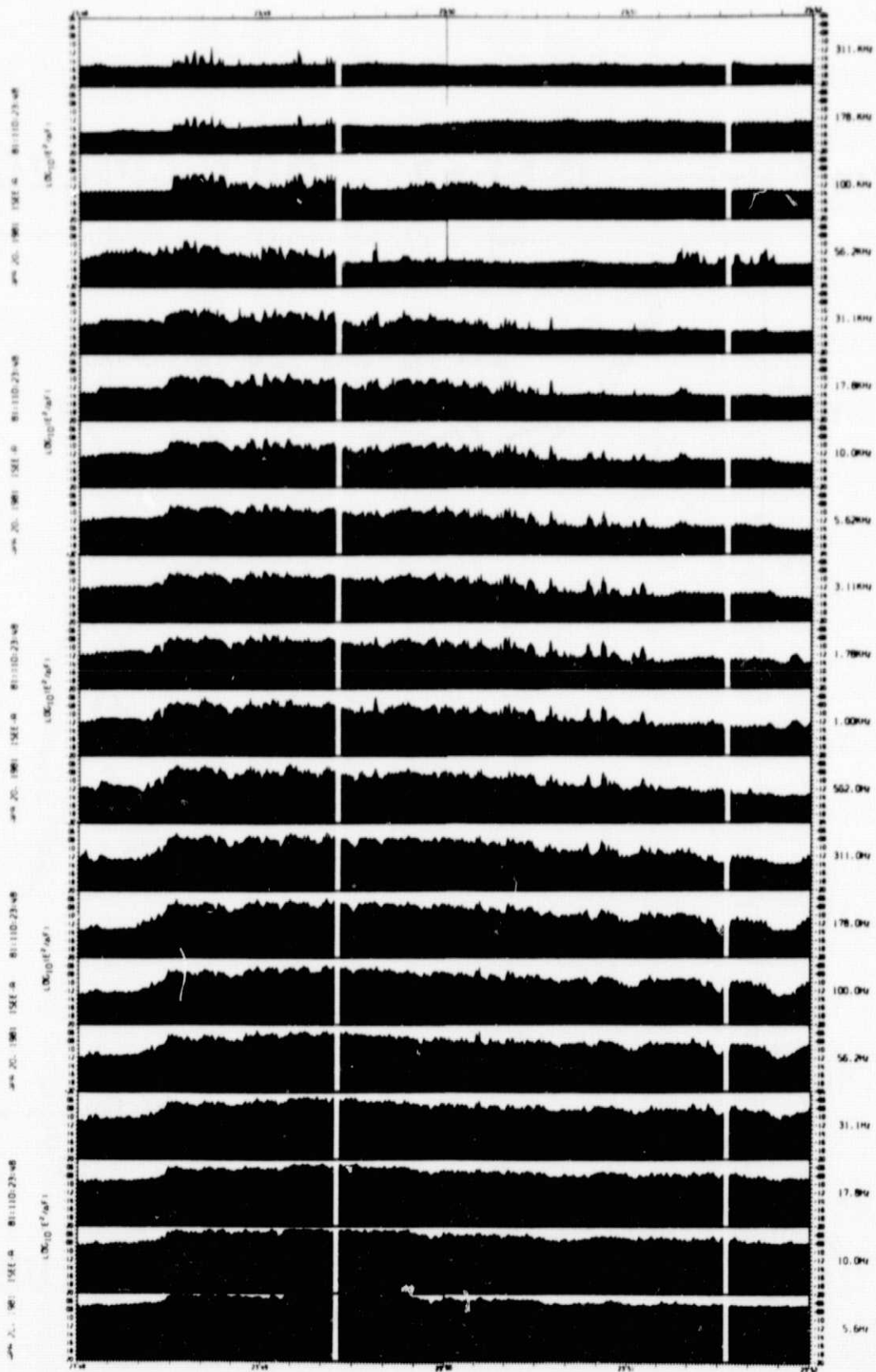
Figure 17

V^2/m^2 Hz   ISEE-1   1981 APR.20

2348:30-2348:33

2348:15-2348:18

FREQUENCY

RMS VALUES

Figure 18

Figure 19

Figure 20

Figure 21